

GW150914-like Black Holes as Galactic High-Energy Sources

Kunihito Ioka,^{1*} Tatsuya Matsumoto,² Yuto Teraki,¹ Kazumi Kashiyama³ and Kohta Murase^{1,4,5,6}

¹Center for Gravitational Physics, Yukawa Institute for Theoretical Physics, Kyoto University, Kyoto 606-8502, Japan

²Department of Physics, Graduate School of Science, Kyoto University, Kyoto 606-8502, Japan

³Department of Physics, University of Tokyo, Bunkyo, Tokyo 113-0033, Japan

⁴Department of Physics, The Pennsylvania State University, University Park, PA 16802, USA

⁵Department of Astronomy & Astrophysics, The Pennsylvania State University, University Park, PA 16802, USA

⁶Center for Particle and Gravitational Astrophysics, The Pennsylvania State University, University Park, PA 16802, USA

Accepted XXX. Received YYY; in original form ZZZ

ABSTRACT

The first direct detections of gravitational waves (GWs) from black hole (BH) mergers, GW150914, GW151226 and LVT151012, give a robust lower limit ~ 70000 on the number of merged, highly-spinning BHs in our Galaxy. The total spin energy is comparable to all the kinetic energy of supernovae that ever happened in our Galaxy. The BHs release the spin energy to relativistic jets by accreting matter and magnetic fields from the interstellar medium (ISM). By considering the distributions of the ISM density, BH mass and velocity, we calculate the luminosity function of the BH jets, and find that they can potentially accelerate TeV–PeV cosmic-ray particles in our Galaxy with total power $\sim 10^{37\pm 3}$ erg s⁻¹ as PeVatrons, positron factories and/or unidentified TeV gamma-ray sources. Additional ~ 300 BH jet nebulae could be detectable by CTA (Cherenkov Telescope Array). We also argue that the accretion from the ISM can evaporate and blow away cold material around the BH, which has profound implications for some scenarios to predict electromagnetic counterparts to BH mergers.

Key words: gravitational waves – stars: black holes – cosmic rays – gamma-rays: general – ISM: jets and outflows – acceleration of particles

1 INTRODUCTION

A century after Einstein predicted the existence of gravitational waves (GWs), the Laser Interferometer Gravitational-Wave Observatory (LIGO) observed the first direct GW signal GW150914 from a merger of two black holes (BHs) with masses of $36_{-4}^{+5}M_{\odot}$ and $29_{-4}^{+4}M_{\odot}$ and radiated energy $3_{-0.4}^{+0.5}M_{\odot}c^2$. (Abbott et al. 2016a). This is also the first discovery of a binary BH. During Advanced LIGO’s first observing period (O1), September 12, 2015 to January 19, 2016 (The LIGO Scientific Collaboration et al. 2016),¹ the second event GW151226 with masses $14.2_{-3.7}^{+8.3}M_{\odot}$ and $7.5_{-2.3}^{+2.3}M_{\odot}$ and radiated energy $1.0_{-0.2}^{+0.1}M_{\odot}c^2$ (Abbott et al. 2016b) and a candidate LVT151012 with $23_{-6}^{+18}M_{\odot}$, $13_{-5}^{+4}M_{\odot}$ and $1.5_{-0.4}^{+0.3}M_{\odot}c^2$ have been also detected, and the exis-

tence of a population of merging BHs has been established. These ~ 2.5 events give a relatively certain estimate on the merger rate in the range $\mathcal{R}_{\text{GW}} \sim 9\text{--}240$ Gpc⁻³ yr⁻¹ (The LIGO Scientific Collaboration et al. 2016). A new era of GW astrophysics has been finally opened and will be driven by a network of LIGO, Virgo, KAGRA, and IndiGO, and by eLISA and DECIGO satellites in the future (Sesana 2016; Kyutoku & Seto 2016; Nakamura et al. 2016b).

The binary BH mergers are the most luminous events in the universe, even brighter than gamma-ray bursts (GRBs). The peak luminosities are $3.6_{-0.4}^{+0.5} \times 10^{56}$ erg s⁻¹, $3.3_{-1.6}^{+0.8} \times 10^{56}$ erg s⁻¹ and $3.1_{-1.8}^{+0.8} \times 10^{56}$ erg s⁻¹ for GW150914, GW151226 and LVT 151012, respectively (The LIGO Scientific Collaboration et al. 2016), which reach $\sim 0.1\%$ of the Planck luminosity $c^5/G = 3.6 \times 10^{59}$ erg s⁻¹ = $2.0 \times 10^5 M_{\odot}c^2$ s⁻¹. Merged BHs also retain

* E-mail: kunihito.ioka@yukawa.kyoto-u.ac.jp (KI)

¹ O1 was officially September 18, 2015 to January 12, 2016 before the detection of GW150914.

huge energy in the spin. The spin energy is about

$$E_{\text{spin}} = \left(1 - \sqrt{\frac{1 + \sqrt{1 - a_*^2}}{2}}\right) Mc^2 \sim 1 \times 10^{54} \text{ erg} \left(\frac{M}{10M_\odot}\right),$$

where the spin parameter is typically $a_* = a/M \sim 0.7$ after a merger (e.g., [Zlochower & Lousto 2015](#)).

Post-merger spinning BHs should also exist in our Galaxy, having a lot of energy in the spin. The number of such BHs is estimated as

$$N_{\text{BH}} \sim \mathcal{R}_{\text{GW}} n_{\text{gal}}^{-1} H_0^{-1} \sim 7 \times 10^4 \text{ galaxy}^{-1} \left(\frac{\mathcal{R}_{\text{GW}}}{70 \text{ Gpc}^{-3} \text{ yr}^{-1}}\right), \quad (2)$$

where we use $\mathcal{R}_{\text{GW}} \sim 70 \text{ Gpc}^{-3} \text{ yr}^{-1}$ ([The LIGO Scientific Collaboration et al. 2016](#)), $n_{\text{gal}} \sim 0.01 \text{ Mpc}^{-3}$ is the number density of galaxies, and $H_0^{-1} \sim 10^{10} \text{ yr}$ is the Hubble time. This estimate is applicable unless the merger rate changes very rapidly in a time much shorter than the Hubble time. Note that, although the large mass in GW150914 suggest a low-metallicity environment with $Z \lesssim Z_\odot/2$ ([Abbott et al. 2016c](#)), our Galaxy had a low-metallicity environment in the past, and also incorporated low-metallicity galaxies in the hierarchical structure formation. The total spin energy stored in the merged BHs in our Galaxy is

$$E_{\text{tot}} = N_{\text{BH}} E_{\text{spin}} \sim 9 \times 10^{58} \text{ erg} \sim 9 \times 10^7 E_{\text{SN}}, \quad (3)$$

where $E_{\text{SN}} \sim 10^{51} \text{ erg}$ is the kinetic energy of a supernova (SN). This is comparable to the total energy of SNe that ever happened in our Galaxy, i.e., $\sim 10^8$ SNe exploded during the Hubble time! This is a robust lower limit on the total spin energy, obtained by the GW observations for the first time.

A natural question arises: How much spin energy is extracted from the merged BHs in our Galaxy? The spin energy of a BH can be extracted by a large-scale poloidal magnetic field threading the BH, i.e., through Blandford-Znajek effect ([Blandford & Znajek 1977](#)), which is thought to produce a BH jet. We show that a sufficient magnetic field is advected by the Bondi-Hoyle accretion from the interstellar medium (ISM) and the jet power becomes comparable to the accretion rate, which is larger than the radiative power of the accretion disk. By taking into account the distributions of the ISM density, the BH mass and velocity, we estimate the luminosity function and the total power of the BH jets.

Based on the estimate of the luminosities and the acceleration energy, we suggest that the BH jets are potentially the origin of high energy particles in our Galaxy. There are enigmatic high-energy sources in our Galaxy, such as still-unknown PeVatrons accelerating cosmic rays (CRs) up to the knee energy $\epsilon_{\text{knee}} \sim 3 \times 10^{15} \text{ eV}$ and beyond, sources of TeV CR positrons, and unidentified TeV sources (TeV unIDs) that are dominant in the very-high-energy gamma-ray sky. These sources require only a small fraction of the spin energy E_{tot} and could be powered by the BH jets.

Our examination of the BH accretion and jet also suggests that it is very difficult to detect an electromagnetic counterpart to a BH merger after a GW event. In particular, the report of a GRB around the time of GW150914 by the Fermi Gamma-ray Burst Monitor (GBM) ([Connaughton et al. 2016](#)) is most likely irrelevant to the GW event. This is consistent with a large number of follow-up searches af-

ter GW150914 ([Ackermann et al. 2016](#); [Kasliwal et al. 2016](#); [Troja et al. 2016](#); [KamLAND Collaboration et al. 2016](#); [Adrián-Martínez et al. 2016](#); [Tavani et al. 2016](#); [Abbott et al. 2016d](#); [Adriani et al. 2016](#); [Evans et al. 2016a](#); [Palliyaguru et al. 2016](#); [The Pierre Auger Collaboration et al. 2016](#); [Abe et al. 2016](#); [Morokuma et al. 2016](#); [Evans et al. 2016b](#)).

The organization of this paper is as follows. In Section 2, we discuss the physical mechanism of energy extraction from a spinning BH. We find that the accretion disk typically results in the so-called magnetically arrested disk (MAD) state and the magnetic field extracts the spin energy with the maximum efficiency for producing a jet. In Section 3, we calculate the luminosity function of the BH jets by considering the distributions of the BH mass, the peculiar velocity, the GW recoil velocity, and the ISM density. The luminosity function also gives the total power of the BH jets. In Section 4, we discuss the connections of the BH jets with high energy sources in our Galaxy, such as PeVatrons, CR positron sources, and TeV unIDs. In Section 5, we encompass the uncertainties of our estimate on the total power within a factor of $10^{\pm 3}$ by taking into account various effects such as the initial spin, the BH formation scenario, and the wind feedbacks. This is much better than before; the factor was almost $10^{\pm \infty}$ before the GW detections. In Section 6, we show that BHs are difficult to keep accretion disks until the merger that are massive enough for making a detectable electromagnetic counterpart for GW150914. Section 7 is devoted to the summary and discussions. In Section A, we clarify novel points of our work compared with previous studies.

2 EXTRACTING SPIN ENERGY OF GW150914-LIKE GALACTIC BHS

The spin energy of a BH can be extracted by a large-scale magnetic field threading the BH ergosphere. The BH spin twists the magnetic field and the twisted magnetic field carries energy outward as a Poynting jet. This is the so-called BZ effect ([Blandford & Znajek 1977](#); [Koide et al. 2002](#)). Although the BH itself cannot keep the magnetic field because of the no-hair theorem, accretion onto the BH can maintain the magnetic field on the BH. In this section we consider a BH in the ISM and estimate the luminosity of a BZ jet powered by the BH spin. For typical parameters, we find that the luminosity of a BH jet is comparable to the accretion rate $L_j \approx \dot{M}c^2$, with the accretion disk in the state of the so-called MAD.

2.1 Bondi accretion from the ISM

The accretion rate onto a BH from the ISM is given by the Bondi-Hoyle rate ([Hoyle & Lyttleton 1939](#); [Bondi & Hoyle 1944](#); [Bondi 1952](#)),

$$\begin{aligned} \dot{M} &= 4\pi r_B^2 V \rho = \frac{4\pi G^2 M^2 n \mu m_u}{V^3} \\ &\sim 5 \times 10^{35} \text{ erg s}^{-1} \frac{1}{c^2} \left(\frac{n}{10 \text{ cm}^{-3}}\right) \left(\frac{M}{10M_\odot}\right)^2 \left(\frac{V}{10 \text{ km s}^{-1}}\right)^{-3} \\ &\sim 4 \times 10^{-4} \frac{L_{\text{Edd}}}{c^2} \left(\frac{n}{10 \text{ cm}^{-3}}\right) \left(\frac{M}{10M_\odot}\right) \left(\frac{V}{10 \text{ km s}^{-1}}\right)^{-3}, \quad (4) \end{aligned}$$

where n is the number density of the ISM, m_u is the unified atomic mass unit, the mean molecular weight is $\mu = 1.41$ for the Milky Way abundance and $\mu = 2.82$ for molecular clouds (e.g., Kauffmann et al. 2008), M is the mass of the merged BH, L_{Edd} is the Eddington luminosity,

$$r_B = \frac{GM}{V^2} \sim 1 \times 10^{15} \text{ cm} \left(\frac{M}{10M_\odot} \right) \left(\frac{V}{10 \text{ km s}^{-1}} \right)^{-2} \quad (5)$$

is the Bondi radius, and

$$V = \sqrt{c_s^2 + v^2 + v_{\text{GW}}^2} \quad (6)$$

includes the (effective) sound speed c_s of the ISM, the center-of-mass velocity v of the BH before the merger in the local ISM, and the recoil velocity v_{GW} due to the GW emission at the merger. The accretion rate \dot{M} is proportional to $M^2 V^{-3} n$. The discovery of a massive BH with mass $M \sim 60M_\odot$ in GW150914 significantly increases the estimate of \dot{M} , while the GW recoil tends to reduce it. The ISM density spans many decades. Thus we have to consider the distributions of mass, velocity, and density to estimate the total power in Section 3.

2.2 Formation of an accretion disk and ADAF

The accreted matter forms an accretion disk for typical parameters (Fujita et al. 1998; Agol & Kamionkowski 2002). The ISM density has a turbulent fluctuation with a Kolmogorov spectrum $\delta\rho/\rho \sim [L/(6 \times 10^{18} \text{ cm})]^{1/3}$ down to $\sim 10^8 \text{ cm}$ (Armstrong et al. 1995; Draine 2011). As a BH travels in the ISM, the accreting matter acquires a net specific angular momentum

$$\ell \sim \frac{1}{4} \frac{\Delta\rho}{\rho} V r_B, \quad (7)$$

where $\Delta\rho/\rho = \delta\rho/\rho|_{L=2r_B}$ is the density difference across the accretion cylinder.² By equating this with the Keplerian angular momentum $\ell_K = \sqrt{GM r_{\text{disk}}}$, we obtain the radius of the resulting accretion disk,

$$\begin{aligned} \frac{r_{\text{disk}}}{r_S} &\sim \frac{1}{16} \left(\frac{2GM/V^2}{6 \times 10^{18} \text{ cm}} \right)^{2/3} \frac{c^2}{2V^2} \\ &\sim 2 \times 10^5 \left(\frac{M}{10M_\odot} \right)^{2/3} \left(\frac{V}{10 \text{ km s}^{-1}} \right)^{-10/3}, \end{aligned} \quad (8)$$

where $r_S = 2GM/c^2$ is the Schwarzschild radius. The disk radius could be decreased if the magnetic breaking is effective.

The accretion disk most likely forms hot, geometrically-thick accretion flow such as advection-dominated accretion flow (ADAF) (Fujita et al. 1998). The accreted matter is heated and eventually ionized because the collisional ionization rate is larger than the accretion rate as well as the recombination rate for typical parameters (see also Section 6). The accretion rate is much lower than the Eddington rate as in Equation (4) and hence the low density makes the cooling ineffective (Ichimaru 1977; Narayan & Yi 1994, 1995; Kato et al. 2008; Yuan & Narayan 2014). The

² A factor 1/4 comes from the average over the accretion cylinder, $\int_0^{r_B} r dr \int_0^{2\pi} d\theta (r \cos\theta)^2 / r_B^2 \int_0^{r_B} r dr \int_0^{2\pi} d\theta = \frac{1}{4}$. If a turbulent velocity dominates V , the factor has a fluctuation depending on the velocity direction.

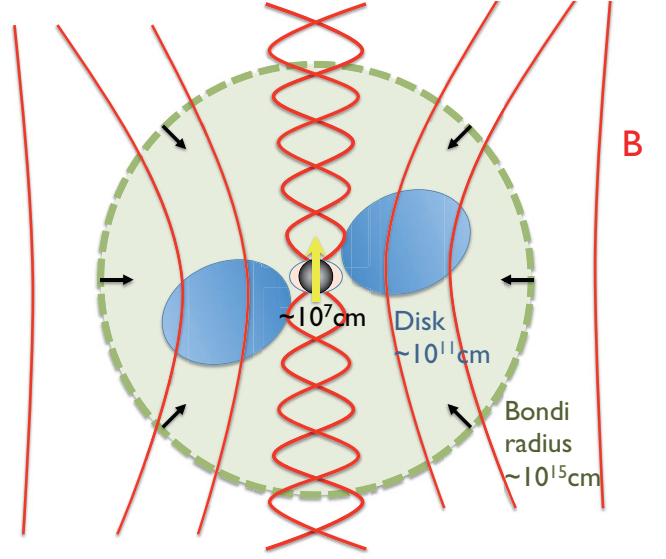


Figure 1. Schematic picture of a Blandford-Znajek jet from a spinning BH that is accreting from the ISM.

radiated energy from ADAF is much less than the total generated energy and almost all energy is advected into the BH (see also Section 5.3). For example, the luminosity of bremsstrahlung emission from electrons is only $L_{\text{brem}} \sim (\alpha_{\text{QED}}/\alpha^2)(m_e/m_u)(\dot{M}c^2/L_{\text{Edd}})\dot{M}c^2 \ll \dot{M}c^2$, where α_{QED} is the fine-structure constant, α is the viscous parameter, and m_e is the electron mass. As shown below, this is much smaller than the jet luminosity. Thus we concentrate on the jet in this paper and consider the disk emission in the future papers (Matsumoto et al. 2016).

A transition to a cold standard disk outside the hot disk is not expected for typical parameters, although this is common in BH X-ray binaries (e.g., Esin et al. 1997; Kato et al. 2008). The reason is that at the initial radius in Equation (8), the disk is already hot (ionized) and the maximum accretion rate of the ADAF solution (Abramowicz et al. 1995) is larger than the accretion rate in Equation (4), i.e., cooling is ineffective. Then we do not also expect soft X-ray transients (or X-ray novae) caused by the accumulation of the accreted matter at some radius because the thermal instability due to recombination is absent for the ionized flow (e.g., Kato et al. 2008).

2.3 Blandford-Znajek jet from a MAD state

The accretion of the ISM also drags magnetic fields into the BH (see Figure 1). The magnetic fields are well frozen in the accreting fluid because the loss time of the magnetic flux in the ISM is much longer than the accretion time (Nakano et al. 2002). The formed disk is also thick, being able to advect the magnetic flux inward (Lubow et al. 1994; Cao 2011). The coherent length of the magnetic field in the ISM is much larger than the Bondi radius, approximately about the scale of energy injection by SNe and stellar winds $\sim 1\text{--}10 \text{ pc}$ (Han et al. 2004). Then the magnetic flux conservation implies the magnetic field strength on the horizon

$$B_H \sim \left(\frac{r_B}{r_H} \right)^2 B_{\text{ISM}}, \quad (9)$$

where B_{ISM} is the magnetic field strength in the ISM, and $r_H = \frac{1}{2} (1 + \sqrt{1 - a_*^2}) r_S$ is the radius of the BH horizon. On the other hand, for a given accretion rate, there is a maximum strength of the magnetic field on the horizon,

$$B_H \sim \sqrt{\frac{4GM\dot{M}}{r^3 v_r}} \Big|_{r=r_H} \sim 4 \times 10^7 \text{ G} \left(\frac{n}{10 \text{ cm}^{-3}} \right)^{1/2} \left(\frac{V}{10 \text{ km s}^{-1}} \right)^{-3/2}, \quad (10)$$

because the pressure of the magnetic field,

$$p_B = \frac{B^2}{8\pi}, \quad (11)$$

can not exceed the ram pressure of the accreting matter,

$$p_a = \frac{GM\Sigma}{r^2} \sim \frac{GMM}{2\pi r^3 v_r}, \quad (12)$$

where $\Sigma = \dot{M}/2\pi r v_r$ is the surface density, $v_r \equiv \varepsilon v_{\text{ff}}$ is the radial velocity, $v_{\text{ff}} = \sqrt{3GM/4\pi r}$ is the free-fall time, and $\varepsilon \sim 0.05$ is suggested by the numerical simulations and observations (Tchekhovskoy et al. 2011; Zamaninasab et al. 2014). Although accumulation of the magnetic flux with the same polarity makes a magnetic barrier (Bisnovatyi-Kogan & Ruzmaikin 1976), the accretion continues through a magnetic flux via magnetic interchange instability (e.g., Arons & Lea 1976; McKinney et al. 2012). Such a magnetically-dominated state is the so-called MAD (Bisnovatyi-Kogan & Ruzmaikin 1976; Narayan et al. 2003; Tchekhovskoy et al. 2011). The MAD state is realized if B_H in Equation (9) is larger than that in Equation (10), i.e.,

$$B_{\text{ISM}} > B_{\text{crit}} \equiv \left(\frac{r_H}{r_B} \right)^2 \sqrt{\frac{4GM\dot{M}}{r^3 v_r}} \Big|_{r=r_H} \sim 1 \times 10^{-10} \text{ G} \left(\frac{V}{10 \text{ km s}^{-1}} \right)^{5/2} \left(\frac{n}{10 \text{ cm}^{-3}} \right)^{1/2} \quad (13)$$

This is usually satisfied for typical $B_{\text{ISM}} \sim 3\mu\text{G}$. Thus the formed disk is likely MAD.

A spinning BH immersed in large-scale poloidal magnetic fields releases energy through the BZ effect with a Poynting luminosity

$$L_j \approx \frac{\kappa}{4\pi c} \Omega_H^2 \Psi_{\text{BH}}^2, \quad (14)$$

where $\kappa \approx 0.05$ (Tchekhovskoy et al. 2011), $\Omega_H = a_* c/2r_H$ is the angular frequency of the BH, and $\Psi_{\text{BH}} \sim \pi r_H^2 B_H$ is a magnetic flux on the BH. For a MAD state $p_B \sim p_a$, the BZ luminosity is calculated as

$$L_j \sim \left(\frac{\kappa}{\varepsilon} \sqrt{\frac{\pi^3}{12}} \frac{r_S}{2r_H} \right) a_*^2 \dot{M} c^2 \approx \dot{M} c^2 \quad (15)$$

for a typical spin parameter after the merger $a_* \approx 0.7$. In the following we will use $L_j \approx \dot{M} c^2$ to estimate the jet luminosity of the merged BHs.³

Note that the net angular momentum direction of the

³ We have confirmed that the results are almost similar even if we use $L_j \approx a_*^2 \dot{M} c^2$.

accretion flow changes on a timescale of crossing the density fluctuation $t_a \sim r_B/V \sim 40 \text{ yr} (M/10M_\odot) (V/10 \text{ km s}^{-1})^{-3}$. However the angular momentum vector near the BH is forced to align with the BH spin by the Bardeen-Petterson effect (Bardeen & Petterson 1975). In addition, although the direction of the poloidal magnetic fields is generally different from the BH spin direction, the magneto-spin alignment is also realized by the frame-dragging effect (McKinney et al. 2013). Therefore we can consider that the direction of the jet is the same as that of the BH spin.

3 LUMINOSITY FUNCTION OF GW150914-LIKE GALACTIC BH JETS

Since the accretion rate depends on nM^2V^{-3} that spans many decades, we calculate the luminosity function of jets from GW150914-like merged BHs in our Galaxy as

$$\frac{dN}{dM} = N_{\text{BH}} \int dm_1 \frac{dp(m_1)}{dm_1} \int dm_2 \frac{dp(m_2|m_1)}{dm_2} \int dv \frac{df(v)}{dv} \times \int dn \frac{d\xi(n)}{dn} h(m_1, m_2, v) \delta[\dot{M}(n, m_1, m_2, v) - \dot{M}] \quad (16)$$

where $dp(m_1)/dm_1$ and $dp(m_2|m_1)/dm_2$ are the distributions of BH masses (Section 3.1), $df(v)/dv$ is the distribution of the pre-merger velocity (Section 3.2), $d\xi(n)/dn$ is the distribution of the ISM density (Section 3.3), and $h(m_1, m_2, v)$ is the correction factor due to the scale heights of the ISM phases and BH distributions (Section 3.4). First, the delta function can be integrated over v analytically as

$$\frac{dN}{dM} = N_{\text{BH}} \int dm_1 \frac{dp(m_1)}{dm_1} \int dm_2 \frac{dp(m_2|m_1)}{dm_2} \int dn \frac{d\xi(n)}{dn} \times h(m_1, m_2, v_0) \frac{df(v_0)}{dv} \frac{V_{v=v_0}^2}{3v_0 \dot{M}}, \quad (17)$$

where $v_0^2 \equiv (4\pi G^2 M^2 n \mu m_u / \dot{M})^{2/3} - c_s^2 - v_{\text{GW}}^2$ should be positive, otherwise the integrand vanishes. The other integrals are computed numerically. We adopt $N_{\text{BH}} \sim 7 \times 10^4$ BHs galaxy⁻¹ as a fiducial value, corresponding to the GW event rate $\mathcal{R}_{\text{GW}} \sim 70 \text{ Gpc}^{-3} \text{ yr}^{-1}$ (The LIGO Scientific Collaboration et al. 2016) in Equation (2).

3.1 Mass function

We assume a Salpeter-like mass function for the primary BH,

$$\frac{dp(m_1)}{dm_1} = C m_1^{-\gamma}, \quad (18)$$

with a uniform distribution of the secondary mass,

$$\frac{dp(m_2|m_1)}{dm_2} = \frac{1}{m_1 - M_{\text{min}}}, \quad (19)$$

where $\gamma = 2.35$, $M_{\text{min}} \leq m_2 \leq m_1 \leq M_{\text{max}}$, $M_{\text{min}} = 5M_\odot$, $M_{\text{max}} = 50M_\odot$, and $C = (\gamma - 1)/(M_{\text{min}}^{1-\gamma} - M_{\text{max}}^{1-\gamma})$. Such mass functions are inferred by the observations of massive stars (Sana et al. 2012; Kobulnicky et al. 2014). Similar mass functions⁴ are adopted by the analysis of LIGO O1 data

⁴ LIGO imposes $m_1 + m_2 < 100M_\odot$ instead of $M_{\text{max}} = 50M_\odot$.

(The LIGO Scientific Collaboration et al. 2016), and are consistent with the GW observations. Note that the total luminosity is dominated by heavy masses for $\gamma < 3$. In this respect, GW150914 is crucial by raising the maximum mass M_{\max} and hence the expected luminosity more than was previously thought (cf. $M_{\max} = 13M_{\odot}$ was adopted in Agol & Kamionkowski (2002)). Note also $\gamma = 0.35$ in Agol & Kamionkowski (2002)).

3.2 Velocity distribution before a merger

The velocity distribution for GW150914-like BHs before mergers is described by a Maxwell-Boltzmann distribution,

$$\frac{df(v)}{dv} = \sqrt{\frac{2}{\pi}} \frac{v^2}{\sigma_v^3} \exp\left(-\frac{v^2}{2\sigma_v^2}\right), \quad (20)$$

where an isotropic Gaussian approximation is enough for our order-of-magnitude estimates. As a fiducial value, we take the velocity dispersion $\sigma_v = 40 \text{ km s}^{-1}$ by considering the isolated binary formation scenario. From a theoretical point of view, massive star progenitors are born from molecular clouds and their velocity dispersion is initially low $\sigma_v \sim 10 \text{ km s}^{-1}$ (Binney & Merrifield 1998). Unless the BH formation is associated with an exceptionally large kick due to such as asymmetric mass ejection, the resulting BHs have also low velocities. If the kick velocity is inversely proportional to the mass following the momentum conservation, the kick velocity of neutron stars implies $\sigma_v \sim 200 \text{ km s}^{-1} (1.4M_{\odot}/M) \sim 30 \text{ km s}^{-1} (M/10M_{\odot})^{-1}$. Older stars tend to have larger velocity dispersion and $\sigma_v = 40 \text{ km s}^{-1}$ is reasonable for progenitors with metallicity $Z \lesssim 0.5Z_{\odot}$ (Binney & Merrifield 1998). From an observational point of view, the rms distance $\sim 410 \text{ pc}$ from the Galactic plane for BH low-mass X-ray binaries, corresponding to a scale height of 290 pc , suggest a velocity dispersion of $\sigma_v \sim 40 \text{ km s}^{-1}$ (White & van Paradijs 1996). Although there are exceptions such as GRO 1655-40 with a peculiar velocity $v \sim -114 \text{ km s}^{-1}$ (Brandt et al. 1995; Mirabel et al. 2002) and XTE J1118+480 with $v \sim 145 \text{ km s}^{-1}$ (Mirabel et al. 2001), two populations likely exist with low and high kick velocities, similarly to neutron stars (Cordes & Chernoff 1998; Pfahl et al. 2002). On the other hand, these observations are not for high-mass systems. In addition, these estimates are subject to systematic errors in the distance (Repetto et al. 2012). The most reliable estimate is based on the astrometric observations (Miller-Jones 2014). Although there is only one sample for a high-mass system, the BH high-mass X-ray binary Cygnus X-1 has a relatively low proper motion $\sim 20 \text{ km s}^{-1}$ (Chevalier & Ilovaisky 1998; Mirabel & Rodrigues 2003; Reid et al. 2011).

We discuss a high-velocity case $\sigma_v = 200 \text{ km s}^{-1}$ later in Section 5.2.

3.3 ISM Density

We consider five phases of the ISM as listed in Table 1; the molecular clouds consisting mostly of H_2 , the cold neutral medium consisting of H_I clouds (cold H_I), the warm neutral medium in thermally equilibrium with cold H_I (warm H_I), the warm ionized medium (warm H_{II}), and the hot ionized medium (hot H_{II}) (Bland-Hawthorn & Reynolds 2000;

Ferrière 2001; Heyer & Dame 2015; Inutsuka et al. 2015). For each phase, we use the probability distribution of the number density,

$$\frac{d\xi(n)}{dn} = D\xi_0 n^{-\beta}, \quad (n_1 < n < n_2) \quad (21)$$

where n_1 , n_2 and β are given in Table 1 (Berkhuijsen 1999), $D = (\beta - 1)/(n_1^{1-\beta} - n_2^{1-\beta})$, and $\xi_0 = \int \frac{d\xi}{dn} dn$ is the volume filling fraction (Scoville & Sanders 1987; Clemens et al. 1988; Agol & Kamionkowski 2002).⁵ Each phase has its scale height H_d in the Galactic disk. We assume that the hot H_{II} phase has a sound velocity $c_s = 150 \text{ km s}^{-1}$ corresponding to a temperature $T \sim 10^6 \text{ K}$, while the other phases have effective $c_s \sim 10 \text{ km s}^{-1}$ (corresponding to $T \sim 2 \times 10^4 \text{ K}$) because these phases (even with $T < 2 \times 10^4 \text{ K}$) have also a turbulent velocity $\sim 10 \text{ km s}^{-1}$ in approximately pressure balance with each other. The parameters in Table 1 are similar to those in Agol & Kamionkowski (2002) (Agol & Kamionkowski 2002).

3.4 Scale height

The BHs have their scale height $H(v_z)$ in the Galactic disk. Each phase of the ISM has also its own scale height H_d in Table 1. Then the number of BHs in each phase is corrected by a factor

$$h(m_1, m_2, v) = \min\left[1, \frac{H_d}{H(v_z)}\right]. \quad (22)$$

For simplicity, we make a one-dimensional analysis of the vertical structure, neglecting the coupling of the vertical and horizontal motions. The scale height $H(v_z)$ is determined by the velocity in the z -direction,

$$\frac{1}{2}v_z^2 = \Phi_z[H(v_z)], \quad (23)$$

where the z -component of the velocity is $v_z^2 = \frac{1}{3}(v^2 + v_{\text{GW}}^2)$ and the gravitational potential in the z -direction,

$$\frac{\Phi_z(z)}{2\pi G} = K\left(\sqrt{z^2 + Z^2} - Z\right) + Fz^2, \quad (24)$$

where $Z \sim 180 \text{ pc}$, $K = 48M_{\odot} \text{ pc}^{-2}$, and $F = 0.01M_{\odot} \text{ pc}^{-3}$ (Kuijken & Gilmore 1989a,b). This simple model is sufficient for our order-of-magnitude estimates.

3.5 GW recoil velocity

Merged BHs receive a recoil due to the anisotropic GW emission (Bonnor & Rotenberg 1961; Peres 1962; Bekenstein 1973). GWs carry linear momentum if two merging BHs have different masses and/or finite spins. Fitting formulas for the recoil velocity are obtained by using numerical simulations in the post-Newtonian-inspired forms (Zlochower & Lousto 2015; Campanelli et al. 2007; Baker et al. 2007). The recoil velocity for a merger of non-spinning BHs is well approximated by

$$v_{\text{GW}} = A\eta^2 \sqrt{1 - 4\eta} (1 + B\eta), \quad (25)$$

where $A = 1.20 \times 10^4 \text{ km s}^{-1}$, $B = -0.93$ (Gonzalez et al. 2007; Fitchett 1983), and $\eta = m_1 m_2 / (m_1 + m_2)^2$ is the symmetric mass ratio. The maximum value is $v_{\text{GW}} \sim 175 \text{ km s}^{-1}$

⁵ For the cases without n_2 in Table 1, we use a delta function.

[t]

Table 1. Five ISM phases. The density distribution from n_1 to n_2 with an index β , the volume filling fraction ξ_0 , the (effective) sound velocity c_s (including the turbulent velocity for cold phases), and the scale height of the disk H_d are shown.

Phase	n_1 [cm $^{-3}$]	n_2 [cm $^{-3}$]	β	ξ_0	c_s [km s $^{-1}$]	H_d
Molecular clouds	10^2	10^5	2.8	10^{-3}	10	75 pc
Cold H $_I$	10	10^2	3.8	0.04	10	150 pc
Warm H $_I$	0.3	–	–	0.35	10	0.5 kpc
Warm H $_{II}$	0.15	–	–	0.2	10	1 kpc
Hot H $_{II}$	0.002	–	–	0.4	150	3 kpc

for $\eta = 0.195$. GW150914 has $\eta \sim 0.247$ and hence $v_{\text{GW}} \sim 61$ km s $^{-1}$, and GW151226 has $\eta \sim 0.226$ and hence $v_{\text{GW}} \sim 150$ km s $^{-1}$. Although we have to extrapolate the formula to small η , this does not affect our result so much.

We do not consider the spin-induced recoil because we are now assuming that the pre-merger spin is low to make a conservative estimate on the released energy from BHs. If the pre-merger spin is high, the pre-merger BHs, which are much more abundant than the merged BHs, can release energy through the BZ mechanism even before the merger without the GW recoil. This case will be discussed in Section 5.1. Current observations of GWs show that the primary BH has a spin of < 0.7 at 90% confidence with no evidence for spins being both large and strongly aligned. For GW151226, the effective spin parameter is $0.21^{+0.20}_{-0.10}$ and may imply spinning BHs (The LIGO Scientific Collaboration et al. 2016). For reference, if the spin parameters parallel to the orbital axis are $a_{*2\parallel} \sim 0.2$ and $a_{*1\parallel} \sim 0$ with the same masses $\eta \sim 1/4$, the recoil velocity is about $v_{\text{GW}} \sim 40$ km s $^{-1}$, while it is $v_{\text{GW}} \sim 260$ km s $^{-1}$ if the in-plane spins are $a_{*2\perp} \sim 0.2$ and $a_{*1\perp} \sim 0$ with the same masses $\eta \sim 1/4$ (Zlochower & Lousto 2015).

3.6 Results of the luminosity function

Figure 2 shows the luminosity function of the BH jets from accreting BHs in our Galaxy for the fiducial case (see Table 2 for the other cases), calculated from Equation (16). Each line corresponds the ISM phase where the BHs reside. As the accretion rate is proportional to the ISM density in Equation (4), the jet luminosity is brighter for BHs in denser ISM such as molecular clouds. On the other hand, brighter jets are rarer because the volume filling fraction of denser medium is smaller in the ISM as in Table 1. We can find that the brightest sources in our Galaxy (with the number $dN/d\log\dot{M} \sim 1$) have $L_j \sim 10^{36}$ erg s $^{-1}$ mostly residing in the cold H $_I$, while fainter sources are more abundant.

The GW recoil effect reduces the luminosity by an order-of-magnitude as we can see from the dotted lines, which are calculated by setting $v_{\text{GW}} = 0$. This reduction is approximately determined by the V^{-3} dependence of the accretion rate in Equation (4) as $\sim (v_{\text{GW}}/\sigma_v)^{-3} \sim (100\text{km s}^{-1}/40\text{km s}^{-1})^{-3} \sim 0.06$. Note also that the luminosity function for the hot H $_{II}$ phase has a peak because this phase has a large c_s and so $V \sim c_s$ has little dispersion.

Figure 3 is the same as Figure 2 but with the vertical axis multiplied by $L_j \sim \dot{M}c^2$. This makes it clear that the most energy is generated by BHs in the cold H $_I$ medium.

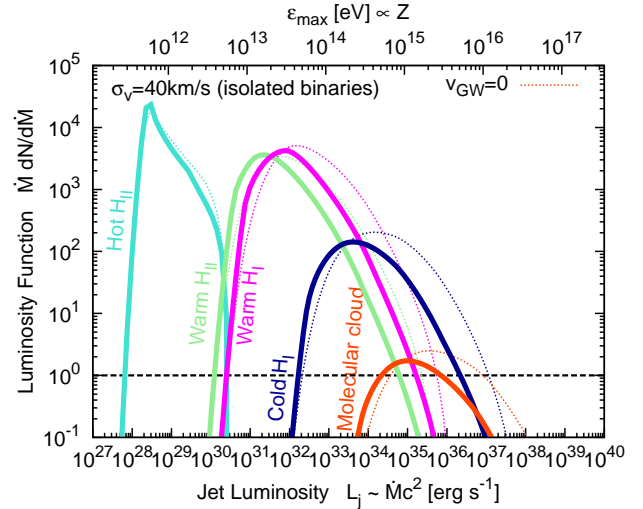


Figure 2. Luminosity function of the BH jets from GW150914-like merged BHs in our Galaxy for the isolated binary formation scenario with the velocity dispersion $\sigma_v = 40$ km s $^{-1}$, calculated from Equation (16). Each line corresponds the ISM phase where the BHs reside (see Table 1). We can see that the most luminous source in our Galaxy has $L_j \sim 10^{36}$ erg s $^{-1}$ for this scenario. Dotted lines are calculated by setting the GW recoil velocity $v_{\text{GW}} = 0$. The upper horizontal axis is the maximum energy of accelerated particles allowed by the Hillas condition for a given luminosity with the charge of accelerated particles $Z = 1$ in Equation (27).

We can read the total power,

$$P_{\text{tot}} = \int L_j \frac{dN}{dM} dM \sim 10^{37} \text{ erg s}^{-1} \left(\frac{N_{\text{BH}}}{7 \times 10^4} \right), \quad (26)$$

which is very roughly derived by $P_{\text{tot}} \sim N_{\text{BH}} \times \xi_0^{\text{H}_I} \times \dot{M}(10\text{cm}^{-3}, 5M_{\odot}, 5M_{\odot}, 100\text{km s}^{-1})c^2 \times (M_{\text{max}}/M_{\text{min}})^{3-\gamma} \sim 7 \times 10^4 \times 0.04 \times 5 \times 10^{32} \text{ erg s}^{-1} \times 4.5 \sim 0.6 \times 10^{37} \text{ erg s}^{-1}$. Note that the velocity dependences of \dot{M} and $f(v)$ cancel with each other and the low velocity BHs have smaller scale height than the cold H $_I$. The total power is approximately $\sim 3 \times 10^{-5}$ of that of SN explosions $E_{\text{SN}}/100\text{yr} \sim 3 \times 10^{41} \text{ erg s}^{-1}$. This is small but comparable to the required power for some high-energy particles in our Galaxy. Based on these results, we will discuss observational implications in the next section.

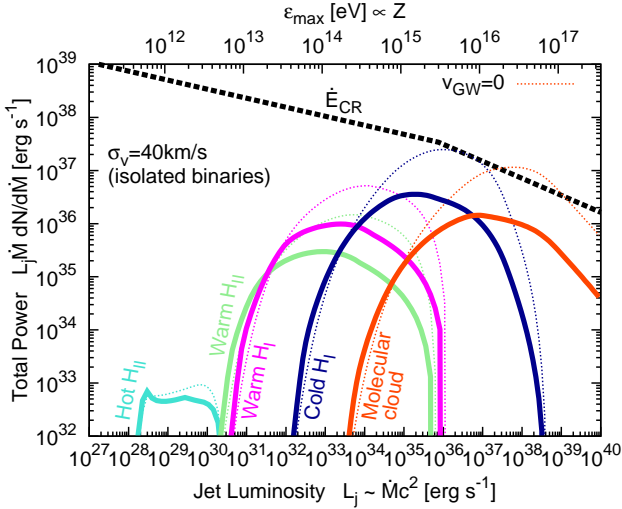


Figure 3. Same as Figure 2 but with the vertical axis multiplied by $L_j \sim M c^2$. We can find that the most energy is generated by BHs in the cold H_I medium. Dashed line plots the required power spectrum for supplying the observed CRs. We can see that the total power is comparable to that of CRs above the knee energy at around ~ 3 PeV within the model uncertainties that are listed in Table 2.

4 OBSERVATIONAL IMPLICATIONS

4.1 PeVatrons

Particle acceleration is ubiquitous in the BH jet system as manifested in active galactic nuclei (AGNs), gamma-ray bursts (GRBs) and X-ray binaries (Longair 2011). The maximum acceleration energy is limited by the source size, i.e., the so-called Hillas condition, $\epsilon_{\max} = ZqBr/\Gamma$, where Z is the charge of accelerated particles, Γ is the Lorentz factor of the acceleration region, and B is the lab-frame magnetic field. This can be written in terms of the Poynting luminosity $L_j \sim 2\pi\theta_j^2 r^2 c(B^2/8\pi)$, where the magnetic field carries an energy density $B^2/8\pi$ at a radius r with the jet opening angle θ_j (Norman et al. 1995; Blandford 2000; Waxman 2004). With the causality condition $\Gamma\theta_j \gtrsim 1$, we have

$$\epsilon_{\max} = ZqB \frac{r}{\Gamma} \sim \frac{2Zq}{\Gamma\theta_j} \sqrt{\frac{L_j}{c}} \lesssim 3.5 \text{ PeV } Z \left(\frac{L_j}{10^{36} \text{ erg s}^{-1}} \right)^{1/2}. \quad (27)$$

Therefore bright sources, i.e., massive BHs in dense ISM, are potential ‘‘PeVatrons’’ accelerating particles beyond PeV energy (Barkov et al. 2012; Kotera & Silk 2016). We plot ϵ_{\max} on the upper horizontal axis in Figures 2 and 3. Possible acceleration sites are discussed in Section 7.

In Figure 3, we also plot the required power spectrum for supplying the observed CRs by using $L_0(\epsilon/\epsilon_{\min}^{\text{CR}})^{2-s} \frac{d\epsilon}{\epsilon} = L_0(\epsilon/\epsilon_{\min}^{\text{CR}})^{2-s} \frac{dM}{2M}$ where the spectral index is $s = 2.34$ below the knee (Genolini et al. 2015)⁶ and 0.3 higher above the knee (Blümer et al. 2009; Gaisser et al. 2013). SN remnants are commonly believed to supply most Galactic CRs from

⁶ The intrinsic spectral index of CRs s is unobservable and different from the observed one by the diffusion coefficient index, which is usually obtained from observations of the boron-to-carbon ratio (Evoli et al. 2015; Oliva 2016; Genolini et al. 2015).

the peak energy $\epsilon_{\min}^{\text{SN}} = 1$ GeV to the knee $\epsilon_{\max}^{\text{SN}} = 3$ PeV. The normalization L_0 is determined by the fact that a fraction $\epsilon_{\text{CR}} = 0.1$ of the SN kinetic energy can yield CRs,

$$\frac{\epsilon_{\text{CR}} E_{\text{SN}}}{100 \text{ yr}} = \int_{\epsilon_{\min}^{\text{SN}}}^{\epsilon_{\max}^{\text{SN}}} L_0 \left(\frac{\epsilon}{\epsilon_{\min}^{\text{SN}}} \right)^{2-s} \frac{d\epsilon}{\epsilon}. \quad (28)$$

From Figure 3 we can see that the BH jets can produce comparable energy to that required for the observed CRs at and beyond the knee energies $\gtrsim 3$ PeV, taking the model uncertainties into account (see Section 5). The origin of these CRs is not known (e.g., Hillas 2005; Blümer et al. 2009; Gaisser et al. 2013). Currently known gamma-ray sources, including even SN remnants, do not show the characteristic PeVatron spectrum extending without a cutoff or break to tens of TeV (Aharonian 2013), with a possible exception of the Galactic center Sagittarius A* (HESS Collaboration et al. 2016). Even if the SN remnants are responsible for CRs up to the knee, the transition from Galactic to extragalactic CRs occurs between the knee and the ankle. Ultra-high-energy CRs above the ankle are extragalactic because of the observed isotropy (Abreu et al. 2010; Abbasi et al. 2016).⁷ If the knee corresponds to the proton cutoff and the source composition is solar, the rigidity-dependent cutoffs extending beyond the knee are not sufficient to fill the observed all-particle flux (Hillas 2005). This implies a second (Galactic) component at energies between the knee and the ankle, sometimes called ‘‘component B’’. Our results suggest that the BH jets might be PeVatrons and/or fill the gap between the knee and the ankle. An unnatural point of this possibility is that the BH jets are totally irrelevant to the SN remnants. It is just a coincidence that the CR fluxes from two kinds of sources are the same within a factor. There are also orders-of-magnitude uncertainties in the estimate of the total power of the BH jets (see Section 5). Furthermore it is difficult to calculate the CR spectrum and the acceleration efficiency at present. Nevertheless the BH jets can potentially accelerate the CRs at and beyond PeV energy with the flux comparable to the observations.

4.2 Cosmic-ray positrons and electrons

The CR positron fraction (the ratio of positrons to electrons plus positrons) has been measured by the PAMELA satellite (Adriani et al. 2009) and more precisely by the AMS-02 experiment (Aguilar et al. 2013). The observed positron fraction rises from ~ 10 GeV at least to ~ 300 GeV, indicating the presence of nearby positron sources within ~ 1 kpc. Although the dark matter annihilation or decay scenario is now severely constrained by other messengers, there are still many astrophysical candidates and the true origin is unclear (e.g., Serpico 2012; Ioka 2010; Kashiyama et al. 2011; Fujita et al. 2009; Kohri et al. 2016).

The BH jets could accelerate electrons and positrons preferentially if the jets are not contaminated by baryons (Barkov et al. 2012) but associated with the pair cascade (see also Section 7). The maximum energy of particle acceleration is enough for producing the observed positrons as

⁷ There could be possible hot spots (Abbasi et al. 2014; Aab et al. 2015).

in Equation (27). The required total power for the positron excess is about $\sim 10^{-4}$ of that of SN explosions, i.e., about $\sim 3 \times 10^{37}$ erg s $^{-1}$. This is comparable to that of the BH jets in Equation (26) within the model uncertainties (see Section 5). Therefore the BH jets are eligible to join the possible sources, although it is again difficult to estimate the spectrum and efficiency of the positron acceleration.

A BH jet likely forms an extended nebula in the ISM, similarly to an AGN cocoon/lobe (Begelman & Cioffi 1989) and a GRB cocoon (Ramirez-Ruiz et al. 2002; Mizuta & Ioka 2013). A BH jet collides with the ISM at the jet head. The shocked matter goes sideways forming a cocoon. Although the cocoon pressure initially collimates the jet, the collimation radius expands and finally reaches the termination (reverse) shock. The maximum size of the termination shock is given by the condition that the jet pressure balances with the ram pressure of the ISM, $L_j/2\pi\theta^2 r_h^2 c \sim n\mu m_u V^2$, i.e.,

$$r_h \sim \sqrt{\frac{L_j}{2\pi\theta^2 c n\mu m_u V^2}} \sim 2 \text{ pc} \left(\frac{L_j}{10^{36} \text{ erg s}^{-1}} \right)^{1/2} \times \left(\frac{n}{10 \text{ cm}^{-3}} \right)^{-1/2} \left(\frac{V}{10 \text{ km s}^{-1}} \right)^{-1} \left(\frac{\theta}{0.1} \right)^{-1}, \quad (29)$$

at which point the jet is completely bent by the ISM and dissipated into the cocoon. The cocoon is also extended along the direction of the proper motion, leading to a more or less spherical shape. The forward shock of the BH jet nebula expands with a velocity $v_c \sim (L_j/n\mu m_u)^{1/5} t^{-2/5}$ and a size $r_c \sim v_c t$, slowing down to $v_c \sim V$ at the maximum size $r_{c,\text{max}} \sim (L_j/n\mu m_u V^3)^{1/2} \sim 80$ pc $(L_j/10^{36} \text{ erg s}^{-1})^{1/2} (n/10 \text{ cm}^{-3})^{-1/2} (V/10 \text{ km s}^{-1})^{-3/2}$. The BH jet nebula is similar to an old pulsar wind nebula (PWN). Then the CR electrons and positrons likely escape from the nebula to the ISM without adiabatic cooling (Kashiyama et al. 2011). Radiative cooling such as synchrotron emission limits the maximum energy of electrons and positrons, which depends on the propagation time and the magnetic field in the nebula (Kawanaka et al. 2010). Future observations beyond TeV energies by CALET, DAMPE and CTA will probe such leptonic PeVatrons (Kobayashi et al. 2004; Kawanaka et al. 2011).

4.3 Unidentified TeV gamma-ray sources

The Galactic Plane survey carried out by HESS led to the discovery of dozens of TeV gamma-ray sources. Among these, the most abundant category is dark accelerators, so-called TeV unidentified sources (TeV unIDs), which have no clear counterpart at other wavelengths (Aharonian et al. 2005, 2006, 2008). They lie close to the Galactic plane, suggesting Galactic sources. Their power-law spectra with an index of 2.1–2.5 imply a connection with CR accelerators. They are extended $\Delta\theta \sim 0.05\text{--}0.3^\circ$, corresponding to a physical size of $\sim 3 \text{ pc} (\Delta\theta/0.2^\circ) (D/\text{kpc})$ for an unknown distance D . Still, their unID nature prevents us to identify their origin (e.g., Yamazaki et al. 2006; de Jager et al. 2009; Ioka & Mészáros 2010).

In Figure 4, we plot the observed flux distribution of the TeV unIDs at energies $\varepsilon_\gamma > 0.2$ TeV in terms of the cumulative number of sources above a flux $N(>F)$, i.e., log

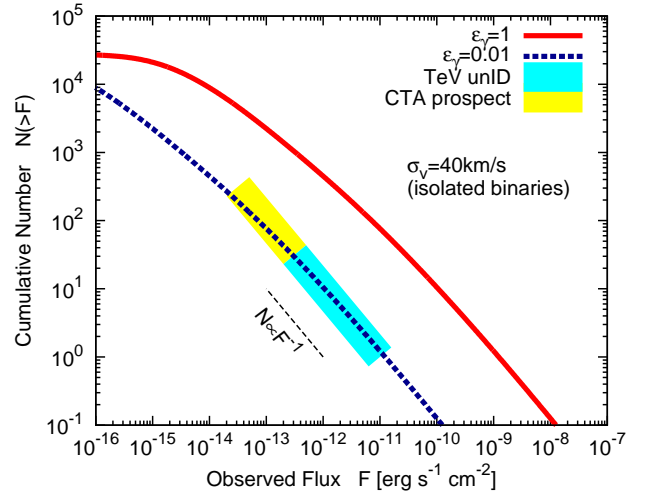


Figure 4. Flux distribution expressed by the cumulative number of sources above a given flux, i.e., $\log N(>F)$ – $\log F$ plot, with Equations (30) and (16). This is compared with the observations of TeV unIDs. Both are comparable if the gamma-ray efficiency is $\varepsilon_\gamma \sim 10^{-2}$. CTA could detect additional ~ 300 BH jets in the near future.

N – $\log F$ plot. In order to compare it with the BH jets, we calculate the flux distribution from the luminosity function in Equation (16) by integrating the number of sources above a given (bolometric) flux $F = L_j/4\pi D^2 \sim \dot{M} c^2/4\pi D^2$ as

$$\frac{dN}{dF} = \int \frac{dN}{dM} \frac{4\pi D^2}{c^2} \frac{DdDd\theta}{\pi R_d^2}, \quad (30)$$

where we approximate the spatial distribution of the BH jets by a thin uniform disk with a radius $R_d = 15$ kpc and the distance of the Sun to the Galactic center $R_\odot = 8$ kpc. A thin approximation is applicable if the observed distance is larger than the scale height ~ 300 pc for the fiducial case (see Table 2).

Figure 4 shows that the flux distribution is comparable with that of TeV unIDs if the gamma-ray efficiency is about $\varepsilon_\gamma \sim 10^{-2}$ for the fiducial parameters (see Table 2). Note that the IC cooling time of 10 TeV electrons is $\sim 10^5$ yr. If the age is $\sim 10^5$ yr, the TeV gamma-ray flux is $\sim 0.1\text{--}0.02 L_e$, implying that $\varepsilon_e \sim 0.1\text{--}0.5$. This is comparable with values considered in GRB jets and PWNs. If this is the case, the CTA (Cherenkov Telescope Array) observatory will increase the number of TeV unIDs up to ~ 300 by improving the sensitivity by about an order of magnitude in the near future (Acharya et al. 2013). Note that the flux distribution follows $N(>F) \propto D^2 \propto F^{-1}$ if the spatial distribution is disk-like, which is different from $N(>F) \propto F^{-1.5}$ for the 3D Euclidian space. The uniform disk approximation is acceptable for the current observations, which have not reached the Galactic center yet. For future observations, we have to consider the high density region near the Galactic center.

The nebular size in Equation (29) is also consistent with the extended nature of TeV unIDs. The BH jet nebula also evades strong upper limits in X-rays with a TeV to X-ray flux ratio up to $\gtrsim 50$ (Matsumoto et al. 2007; Bamba et al. 2007; Matsumoto et al. 2008; Bamba et al. 2009; Fujinaga et al. 2011; Sakai et al. 2011). This is be-

cause the physical parameters such as the energy density and the magnetic field are similar to those of an old PWN. Their emission spectra have the unID nature thanks to the old age (Yamazaki et al. 2006; de Jager et al. 2009; Ioka & Mészáros 2010). In addition, the ADAF disk is radiatively inefficient. The X-ray flux of the ADAF disk is about $F_V \sim (\alpha_{\text{QED}}/\alpha^2)(m_e/m_u)(\dot{M}c^2/L_{\text{Edd}})\dot{M}/4\pi D^2 m_e \sim 1 \times 10^{-18} \text{ erg s}^{-1} \text{ cm}^{-2} \text{ keV}^{-1} (\alpha/0.1)^{-2} (n/10 \text{ cm}^{-3})^2 (M/10M_\odot)^3 (V/10 \text{ km s}^{-1})^{-6} (D/\text{kpc})^{-2}$, below the current limit.

5 MODEL UNCERTAINTIES

Although the GW observations significantly narrow down the possible parameter space, in particular putting a lower bound on the number of spinning BHs in Equation (2), there are still large uncertainties about the model parameters and the estimate for the BH jet power. In this section, we clarify the range of the uncertainties by considering four representative effects: the initial BH spin (Section 5.1), the velocity distribution depending on the binary BH formation scenario (Section 5.2), the accretion rate profile changed by the disk wind (Section 5.3), and the feedback on the ISM by the outflow (Section 5.4). These effects on the model parameters and the resulting total power are summarized in Table 2. We enclose the uncertainty of the total power for the BH jets within a factor of $10^{\pm 3}$, which is much better than before.

5.1 Initial spin

If BHs have spins before the mergers, the BHs can launch BZ jets without the mergers. Such spinning BHs could result from the massive stellar collapse. The total number of BHs in our Galaxy is about $N_{\text{BH}} \sim 10^8$ (Shapiro & Teukolsky 1983), $\sim 10^3$ times larger than that of the merged BHs in Equation (2).⁸ In addition the GW recoil is absent without a merger, increasing the total power by a factor of ten as shown in Figure 3. Then the total power is larger than the fiducial value by a factor of $\sim 10^4 (a_*^i/0.7)^2$ altogether, that is, $P_{\text{tot}} \sim 10^{41} \text{ erg} (a_*^i/0.7)^2$, where the $(a_*^i)^2$ dependence comes from that of the BZ luminosity in Equation (14).

GW observations show no evidence for large spins. Probably the initial spin would be small for most BHs because the massive star progenitors with solar metallicity lose the angular momentum by stellar wind (Heger et al. 2003; Hirschi et al. 2005). Because of the same reason, the BH mass is also smaller than the fiducial case (Abbott et al. 2016c), reducing the total power of the BH jets. In low metallicity, the wind is weak and the resulting BH spin may be high (Yoon & Langer 2005; Hirschi et al. 2005; Kinugawa et al. 2016a). A rapid rotation of the progenitors could lead to a chemically homogeneous evolution without a common envelope phase, avoiding a merger before the BH formation (Mandel & de Mink

2016; Marchant et al. 2016). However the number of such BHs is much less than $N_{\text{BH}} \sim 10^8$. The event rate of GRBs, which likely produce spinning BHs, is comparable to that of the BH mergers. Although some BHs in X-ray binaries might have high spins, these measurements are subject to systematic errors (Remillard & McClintock 2006). For GW151226, the effective spin parameter is $0.21_{-0.10}^{+0.20}$ (The LIGO Scientific Collaboration et al. 2016). So we tentatively take $a_*^i \sim 0.2$ as an upper limit in Table 2. This is the most extreme case because the total power is comparable to that of SN explosions, $E_{\text{SN}}/100 \text{ yr} \sim 3 \times 10^{41} \text{ erg s}^{-1}$.

5.2 Binary BH formation scenario

The accretion rate and the resulting jet luminosity sensitively depend on the velocity of the BH in Equation (4). We have adopted $\sigma_v = 40 \text{ km s}^{-1}$ as a fiducial value for the isolated binary formation scenario (Tutukov & Yungelson 1993; Dominik et al. 2015; Belczynski et al. 2016; Lipunov et al. 2016) in Equation (20).

The GW150914 masses favor low metallicity below $0.5Z_\odot$ (Abbott et al. 2016c). The extreme case is zero metallicity Population III stars (Kinugawa et al. 2014, 2016b,c,a). If BHs form in very low metallicity $< 0.01Z_\odot$, the GW events may be dominated by recent BH mergers in dwarf galaxies (Lamberts et al. 2016) because the low metallicity allows a small initial separation of a BH binary. Then the merged, spinning BHs are incorporated into our Galaxy relatively recently, joining in the halo component with a velocity dispersion of $\sigma_v \sim 200 \text{ km s}^{-1}$.

Another scenario is the dynamical binary formation in a dense stellar cluster (Kulkarni et al. 1993; Sigurdsson & Hernquist 1993; Portegies Zwart & McMillan 2000; Rodriguez et al. 2015, 2016; Mapelli 2016). In a high-density stellar environment, BHs dynamically interact and form binaries. Since the interaction is frequent in the clusters, most of the BH mergers may occur outside the clusters following dynamical ejection. The escape velocity of the clusters is smaller than that of our Galaxy. Thus the merged BHs are floating in our halo with a velocity dispersion of $\sigma_v \sim 200 \text{ km s}^{-1}$.

Primordial BHs are also a possible candidate (e.g., Bird et al. 2016; Sasaki et al. 2016; Nakamura et al. 1997; Ioka et al. 1998, 1999), although this scenario requires a fine tuning in the primordial density fluctuation. In this case, the BHs reside in our halo with $\sigma_v \sim 200 \text{ km s}^{-1}$.

Figure 5 shows the case of $\sigma_v \sim 200 \text{ km s}^{-1}$. Compared with the fiducial case $\sigma_v \sim 40 \text{ km s}^{-1}$ (gray dashed line), the luminosity and hence the total power are reduced by a factor of $\sim 10^2$. This factor is roughly given by the velocity dependence of the accretion rate, $\sim (40 \text{ km s}^{-1}/200 \text{ km s}^{-1})^3 \sim 0.008$. The GW recoil effect becomes less significant than the fiducial case because the velocity dispersion is comparable with the recoil velocity.

5.3 Wind

It remains highly uncertain how much of the accreting matter at the Bondi radius reaches the BH (Yuan & Narayan 2014). Some supermassive BH systems with jets seem to

⁸ The number would be $N_{\text{BH}} \sim 10^{10}$ if dark matter were composed of primordial BHs that are relevant to GWs, while it is suggested that the fraction of primordial BHs in dark matter is small $\sim 10^{-4}$ by observations of GWs and CMB spectral distortion (Sasaki et al. 2016).

Table 2. Possible uncertainties of the model parameters and the resulting total power P_{tot} are summarized. The isolated binary formation scenario is the fiducial case. The column with “–” equals the fiducial value. The model parameters are the number of BH jets N_{BH} , the dispersion of the velocity distribution σ_v in Equation (20), the initial BH spin a_*^i , the accretion rate profile s in Equation (31), and the duty cycle \mathcal{D} reduced by the feedback on the ISM by the disk outflow.

	Number N_{BH}	Velocity σ_v [km s $^{-1}$]	Spin a_*^i	Disk s	Duty cycle \mathcal{D}	Total power P_{tot} [erg s $^{-1}$]
Isolated binary (fiducial)	7×10^4	40	0	0	1	$\sim 10^{37}$
High spin	10^8	–	0.2	–	–	$\sim 10^{37} \times 10^3$
Stellar cluster	–	200	–	–	–	$\sim 10^{37} \times 10^{-2}$
Wind	–	–	–	1	–	$\sim 10^{37} \times 10^{-2}$
Feedback	–	–	–	1	10^{-1}	$\sim 10^{37} \times 10^{-3}$

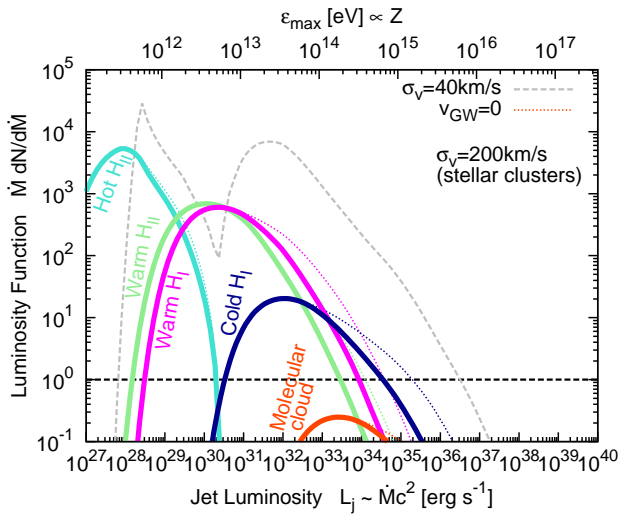


Figure 5. Same as the fiducial case in Figure 2 except for the dispersion of the velocity distribution $\sigma_v = 200$ km s $^{-1}$. The total luminosity function for the fiducial case $\sigma_v = 40$ km s $^{-1}$ is also plotted by a gray dashed line.

require the Bondi accretion rates calculated from the observed gas temperature and density to power the observed jets (Allen et al. 2006; Rafferty et al. 2006; Russell et al. 2013). On the other hand, the ADAF model implies positive Bernoulli parameter for the inflow in the self-similar regime, which suggests that hot accretion flows could have outflows (Narayan & Yi 1994, 1995). The mass outflows make the accretion profile decrease inward approximately in a power-law form, $\dot{M}(r) = \dot{M}(r_{\text{disk}})(r/r_{\text{disk}})^s$, as in the adiabatic inflow-outflow solutions (ADIOS) model (Blandford & Begelman 1999, 2004). The index is limited to $0 \leq s < 1$ by the mass and energy conservation, but has not been determined yet (Yuan & Narayan 2014). The least accretion case corresponds to $s \approx 1$. Recent 3D general relativistic MHD simulations suggest that $s \approx 1$ continues down to $20r_S$, below which the mass flux is constant $s = 0$ (Yuan et al. 2015). This is also implied by an analytical study (Begelman 2012). If we adopt this least accretion case, the accretion rate of the BH is given by

$$\dot{M}_{\text{BH}} \approx \dot{M} \left(\frac{20r_S}{r_{\text{disk}}} \right)^s, \quad \text{if } r_{\text{disk}} > 20r_S, \quad (31)$$

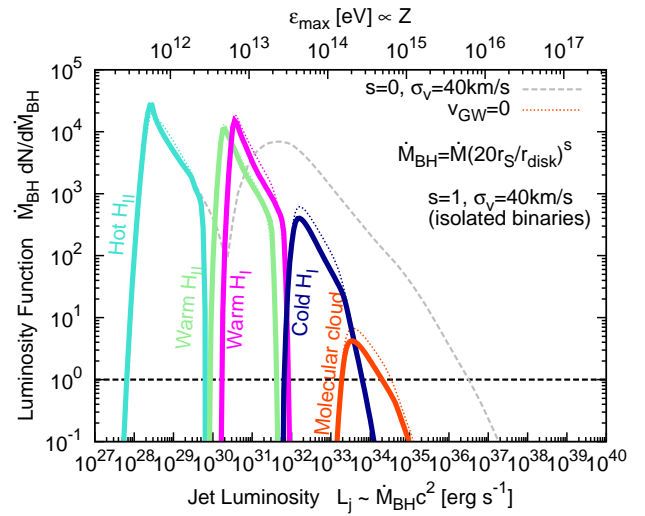


Figure 6. Same as the fiducial case in Figure 2 except for the accretion rate of the BH $\dot{M}_{\text{BH}} = \dot{M}(20r_S/r_{\text{disk}})^s$ with $s = 1$, which is reduced by the wind. The total luminosity function for the fiducial case $s = 0$ is also plotted by a gray dashed line.

with $s \approx 1$ where the disk radius r_{disk} is given by Equation (8). Correspondingly, the luminosity of the BH jet is reduced by the same factor $(20r_S/r_{\text{disk}})^s$.

Figure 6 shows the luminosity function using the accretion rate of a BH in Equation (31). Compared with the fiducial case $s = 0$ (gray dashed line), the luminosity and the total power are reduced by a factor of hundred. This factor is roughly given by the ratio $r_{\text{disk}}/20r_S$ in Equation (8). The GW recoil effect becomes less significant than the fiducial case because the disk radius r_{disk} and the accretion rate \dot{M} have similar dependences on the velocity.

5.4 Feedback

Feedback from radiation, jets and winds on the surrounding ISM could be crucial for estimating the total power of the BH jets, as frequently argued in the context of supermassive BHs (Yuan & Narayan 2014). In the Galactic BH case, the radiative feedback is weak because the ADAF disk is much fainter than the Eddington luminosity. The radiation may ionize the ISM around the Bondi radius, but once ionized, the cross section for the interaction between the ISM and photons decreases by many orders of magnitude,

reducing the radiative feedback. The jet feedback is also not strong because, although the jet dominates the energy output, its penetration ability makes the dissipation scale large as shown in Equation (29). A large amount of ISM is capable of radiating the injected energy.

The most influential feedback would be due to the wind from the disk, if it exists. If the wind is efficient with $s \approx 1$ in Equation (31), even a small efficiency of the wind feedback $\epsilon_w \gtrsim 10^{-6}(M/10M_\odot)^{2/3}(V/10\text{km s}^{-1})^{-4/3}$ is able to heat the ISM at the Bondi radius to blow away, $\epsilon_w \dot{M}_{\text{BH}} c^2 > \dot{M} V^2$. A larger efficiency $\epsilon_w \sim 0.03\text{--}0.001$ is implied by simulations (Sądowski et al. 2016; Yuan et al. 2015; Ohsuga & Mineshige 2011). On the other hand, the wind will stop if the mass accretion at the Bondi radius is terminated. Therefore we expect that the BH activity is intermittent with some duty cycle \mathcal{D} if the wind feedback exists.

A rough estimate of the duty cycle is as follows. The wind is somewhat collimated initially when it is released from the disk. If it were spherical, the wind would not be launched because the ram pressure of the Bondi accretion onto the disk exceeds that of the wind. The 4π solid angle of the ISM is affected by the wind after the wind is decelerated by the ISM, which will happen outside the Bondi radius because the ram pressure of the accretion is a decreasing function of the radius and the wind goes straight inside the Bondi radius. Thus the accretion continues at least for the dynamical time at the Bondi radius,

$$t_a = \frac{r_B}{V} \sim 40 \text{ yr} \left(\frac{M}{10M_\odot} \right) \left(\frac{V}{10\text{km s}^{-1}} \right)^{-3}. \quad (32)$$

The injected energy during the active time is about

$$E_a = \epsilon_w \dot{M}_{\text{BH}} c^2 t_a \sim 3 \times 10^{40} \text{ erg} \left(\frac{\epsilon_w}{3\%} \right) \left(\frac{n}{10\text{cm}^{-3}} \right) \times \left(\frac{M}{10M_\odot} \right)^{11/3} \left(\frac{V}{10\text{km s}^{-1}} \right)^{-8/3}. \quad (33)$$

The injected energy produces a wind remnant and the lifetime of the remnant is about $t_{\text{merge}} \sim t_{\text{PDS}} \times 153 (E_{51}^{1/14} n_0^{1/7} / V_6)^{10/7} \sim 2 \times 10^6 \text{ yr}$ $E_{51}^{3/14} n_0^{-4/7} (E_{51}^{1/14} n_0^{1/7} / V_6)^{10/7}$ according to the notation in Cioffi et al. (1988), which gives

$$t_{\text{merge}} \sim 300 \text{ yr} \left(\frac{E_a}{10^{40} \text{ erg}} \right)^{31/98} \left(\frac{n}{10\text{cm}^{-3}} \right)^{-18/49} \times \left(\frac{V}{10\text{km s}^{-1}} \right)^{-10/7}. \quad (34)$$

Therefore the duty cycle is roughly

$$\mathcal{D} \sim \frac{t_a}{t_{\text{merge}}} \sim 0.1 \left(\frac{V}{10\text{km s}^{-1}} \right)^{-0.73} \times \left(\frac{n}{10\text{cm}^{-3}} \right)^{-0.051} \left(\frac{M}{10M_\odot} \right)^{-0.16}. \quad (35)$$

We use $\mathcal{D} \sim 10^{-1}$ in Table 2.

6 ON FERMI GBM EVENTS ASSOCIATED WITH GW150914

The Gamma-ray Burst Monitor (GBM) on board the Fermi satellite reported a 1 sec-lasting weak GRB 0.4 seconds after GW150914. Assuming the redshift of GW150914, $z =$

$0.09_{-0.04}^{+0.03}$, the luminosity in 1 keV–10 MeV is $1.8_{-1.0}^{+1.5} \times 10^{49} \text{ erg s}^{-1}$ (Connaughton et al. 2016). This was unexpected and prompted many theoretical speculations (Loeb 2016; Zhang 2016; Perna et al. 2016; Li et al. 2016; Veres et al. 2016; Cardoso et al. 2016; Kimura et al. 2016). The anti-coincidence shield (ACS) of the Spectrometer on board INTEGRAL (SPI) put upper limits on the gamma-ray emission with similar fluxes (Savchenko et al. 2016). The GBM result also depend on the analysis of low count statistics (Greiner et al. 2016). No counterpart is observed for GW151226 and LVT151012 (Racusin et al. 2016). Future follow-ups would be finally necessary to confirm or defeat the GBM detection (Yamazaki et al. 2016; Morsony et al. 2016; Murase et al. 2016).

If the signal were caused by the merged BH, the BH would be surrounded by matter. The size of the matter distribution is $r_m \sim 1 \times 10^8 \text{ cm}$ so that the accretion time is

$$t_{\text{acc}} = \frac{1}{\alpha \Omega_K} \left(\frac{r_m}{H} \right)^2 \sim 1.4 \text{ sec} \left(\frac{\alpha}{0.1} \right)^{-1} \left(\frac{M}{60M_\odot} \right)^{-1/2} \times \left(\frac{r_m}{1 \times 10^8 \text{ cm}} \right)^{3/2} \left(\frac{H/r_m}{0.3} \right)^{-2}, \quad (36)$$

where α is the viscosity parameter, H is the disk scale height, and $\Omega_K = \sqrt{GM/r_m^3}$ is the Kepler rotation frequency. The mass of the matter should be larger than $M_m \gtrsim 10^{-5} \theta_j^2 M_\odot$ where θ_j is the opening angle of the GRB jet.

The accretion from the ISM affects the matter surrounding a BH. In particular, it can evaporate a possible dead disk which were invoked for the GBM event (Perna et al. 2016; Kimura et al. 2016). A dead disk is assumed to be cold and neutral due to the small mass, suppressing the magnetorotational instability and hence the viscosity, and remains unaccreted, keeping matter for producing the gamma-ray event. However the accretion from the ISM forms a hot disk sandwiching the dead disk and heating its surface.⁹ The surface temperature develops a gradient, being greater than $T \gtrsim 10^4 \text{ K}$ (corresponding to the sound velocity $v_i \sim \sqrt{k_B T / m_u} \sim 10 \text{ km s}^{-1}$) for the ionized atmosphere. The density n_i at the base of the ionized atmosphere is determined by the pressure balance $n_i v_i^2 \sim n(r) v_h^2$ where $n(r) \sim n(r_B/r)^{3/2}$ and $v_h \sim \sqrt{GM/r}$ are the density and the thermal velocity of the hot disk. Given n_i and v_i , we can estimate the mass evaporation rate (cf. Hollenbach et al. 1994) from the dead disk as

$$\dot{M}_{\text{eva}} \sim 2\pi r^2 n_i v_i m_u \sim 1 \times 10^{15} \text{ g s}^{-1} \left(\frac{r}{10^{12} \text{ cm}} \right)^{-5/2} \times \left(\frac{M}{60M_\odot} \right)^4 \left(\frac{n}{1\text{cm}^{-3}} \right)^{5/2} \left(\frac{V}{40\text{km s}^{-1}} \right)^{-9/2}. \quad (37)$$

Then the evaporation time of the dead disk with mass M_m is

$$t_{\text{eva}} \sim 10^6 \text{ yr} \left(\frac{M_m}{10^{-5} M_\odot} \right) \left(\frac{r}{10^{12} \text{ cm}} \right)^{5/2} \left(\frac{M}{60M_\odot} \right)^{-4} \times \left(\frac{n}{1\text{cm}^{-3}} \right)^{-5/2} \left(\frac{V}{40\text{km s}^{-1}} \right)^{9/2}, \quad (38)$$

which is shorter than $\sim 10^{10} \text{ yr}$, the merger time of the BH

⁹ Note that the accretion does not stop even onto a binary because the disk is thick.

binary with a separation $r \sim 10^{12}$ cm, for the fiducial case. One should keep in mind that the above equation is rather sensitive to parameters M , n and V . For example, BH binaries could have a dead disk if they are formed in a low-density environment. However, for typical parameters, the merged BH would not have a dead disk, implying that the GBM event is not related with GW 150914 in the dead disk scenario.

We can also make a second argument that a time-reversal of this event seems to encounter physical difficulty. Let's go back in time, say $t_b \sim 1000$ sec before the merger. Still the two BHs should be surrounded by the matter. The size of the matter distribution should be larger $r_m \sim 10^{10} \text{ cm} (t_b/10^3 \text{ sec})^{2/3} (\alpha/0.1)^{2/3} (M/60M_\odot)^{1/3} (H/r_m/0.3)^{4/3}$, otherwise the matter is swallowed by the BHs before the merger. The bounding energy of this matter is only a fraction of the rest mass energy of the matter,

$$\frac{GMM_m/r_m}{M_m c^2} \sim 10^{-3} \left(\frac{t_b}{10^3 \text{ sec}} \right)^{-2/3} \left(\frac{\alpha}{0.1} \right)^{-2/3} \times \left(\frac{M}{60M_\odot} \right)^{2/3} \left(\frac{H/r_m}{0.3} \right)^{-4/3}. \quad (39)$$

This ratio is much smaller than the wind efficiency $\epsilon_w \sim 0.1$ of a super-Eddington accretion disk, so that such matter is easily blown away by the disk wind. As long as a possible dead disk is ionized by the ISM accretion (that occurs unless we consider low n and high V), we have encountered an unlikely setup. Note that a fraction of the matter M_m should accrete onto the BHs before the merger, otherwise a fine-tuning is needed because the time t_b is much larger than the event duration t_{acc} . The accretion is super-Eddington, even if only a fraction of the matter accretes, and should be accompanied by a strong disk wind as suggested by numerical simulations (Ohsuga et al. 2005; Jiang et al. 2014; Sądowski et al. 2014). Therefore it is difficult to keep the matter near the BH before the merger and the BH mergers unlikely accompany observable prompt electromagnetic counterparts.

7 SUMMARY AND DISCUSSIONS

We suggest possible connections between the BH mergers observed by GWs and the high energy sources of TeV-PeV particles in our Galaxy. The GW observations give a lower limit on the number of merged and hence highly-spinning BHs as $\sim 70000 (\mathcal{R}_{\text{GW}}/70 \text{ Gpc}^{-3} \text{ yr}^{-1})$, and the spinning BHs produce relativistic jets by accreting matter and magnetic fields from the ISM. We calculate the luminosity function, the total power, and the maximum acceleration energy of the BH jets, and find that the BH jets are eligible for PeVatrons, sources of CR positrons, and TeV unIDs. The BH jets form extended nebulae like PWNe. If they are observed as TeV unIDs, additional ~ 300 nebulae will be discovered by CTA.

We quantify the uncertainties of the estimate for the total power of the BH jets within a factor of $10^{\pm 3}$, which is much better than before the GW detections, by considering the initial BH spin, the velocity distribution depending on the formation scenario, the accretion profile changed by the wind, and the feedback by the outflow (Table 2). The uncertainties will be reduced by the GW observations, in particular, of the BH spins. It is also important to clarify

the feedback by the wind from the sub-Eddington accretion disk on the Bondi-Hoyle accretion.

Our considerations on the BH accretion and jet imply that the electromagnetic counterparts to BH mergers including the Fermi GBM event after GW150914 are difficult to detect with the current sensitivity. The accretion from the ISM can evaporate the cold neutral dead disk around the BH. A slight accretion before the merger can also blow away the surrounding matter if any. These should be considered as constraints on dead disk models for prompt electromagnetic counterparts of the BH-BH merger.

Although we do not go into detail in this paper, there are several sites of particle acceleration for a BH jet. First, the BH magnetosphere acts as a particle accelerator like pulsars if a gap arises with an electric field along the magnetic field (Hirotani et al. 2016; Hirotani & Pu 2016). The gamma-ray emission associated with leptonic acceleration may be detectable for nearby sources although its luminosity is usually much smaller than the BZ luminosity. Second, the internal shocks in the jet are possible like GRBs and AGNs. As long as $B \propto \Gamma/r$ during the propagation, the maximum acceleration energy is the same as Equation (27). Third, the jet dissipates the magnetic energy when the MHD approximation breaks down. This happens when the plasma density drops below the Goldreich-Julian density (Goldreich & Julian 1969), which is the minimum density required for shielding the electric field. The comoving plasma density is given by $n'_p \sim L/4\pi r^2 m_u c^3 \Gamma^2 (1 + \sigma)$ where $L\sigma/(1 + \sigma)$ is the BZ luminosity in Equation (14), σ is the ratio of the Poynting to particle energy flux, Γ is the Lorentz factor of the jet, and we should make an appropriate correction if jets are leptonic. The comoving Goldreich-Julian density beyond the light cylinder $r_\ell = c/\Omega_H = 2r_H/a_*$ is $n'_{\text{GJ}} \sim (\Omega_H/2\pi qc)(r_H/r_\ell)^3 (r_\ell/r\Gamma)$. By equating n'_p with n'_{GJ} , we obtain the radius at which the MHD breaks down,

$$r_{\text{MHD}} \sim \sqrt{\frac{\pi \kappa L}{\sigma(1 + \sigma)c} \frac{q}{m_u c^2} \frac{r_H}{a_*^2 \Gamma}} \sim 2 \times 10^{13} \text{ cm} [\sigma(1 + \sigma)]^{-1/2} \times a_*^{-2} \Gamma^{-1} \left(\frac{L}{10^{35} \text{ erg s}} \right)^{1/2} \left(\frac{M}{10M_\odot} \right). \quad (40)$$

Forth, the termination (reverse) shock of the jet at the radius in Equation (29) is also a plausible site like a hot spot of AGNs and a pulsar wind nebula for pulsars. The jet could be subject to instability, injecting energy into a cocoon/lobe before reaching the termination shock. The shocks between the cocoon and the ISM are also possible sites of particle acceleration. Note that the BH Cygnus X-1 is surrounded by a ring-like structure in radio, which may be formed by the interaction between a jet/cocoon and the ISM (Gallo et al. 2005).

We do not discuss the disk emission in detail. Nearby BH disks with bremsstrahlung, synchrotron, and inverse Compton emission could be detected in the future surveys (Matsumoto et al. 2016). The accretion disks could also accelerate nonthermal particles and contribute to the observed cosmic rays (Teraki et al. 2016). An on-axis BH jet may be also observable if the beaming factor is larger than ~ 0.01 . These are interesting future problems.

ACKNOWLEDGEMENTS

We thank Takashi Nakamura, Tsvi Piran, and Masaru Shibata for helpful comments. This work is supported by KAKENHI 24103006, 24000004, 26247042, 26287051 (K.I.).

REFERENCES

Aab A., et al., 2015, *ApJ*, **804**, 15
 Abbasi R. U., et al., 2014, *ApJ*, **790**, L21
 Abbasi R. U., et al., 2016, preprint, ([arXiv:1608.06306](https://arxiv.org/abs/1608.06306))
 Abbott B. P., et al., 2016a, *Physical Review Letters*, **116**, 061102
 Abbott B. P., et al., 2016b, *Physical Review Letters*, **116**, 241103
 Abbott B. P., et al., 2016c, *ApJ*, **818**, L22
 Abbott B. P., et al., 2016d, *ApJ*, **826**, L13
 Abe K., et al., 2016, preprint, ([arXiv:1608.08745](https://arxiv.org/abs/1608.08745))
 Abramowicz M. A., Chen X., Kato S., Lasota J.-P., Regev O., 1995, *ApJ*, **438**, L37
 Abreu P., et al., 2010, *Astroparticle Physics*, **34**, 314
 Acharya B. S., et al., 2013, *Astroparticle Physics*, **43**, 3
 Ackermann M., et al., 2016, *ApJ*, **823**, L2
 Adrián-Martínez S., et al., 2016, *Phys. Rev. D*, **93**, 122010
 Adriani O., et al., 2009, *Nature*, **458**, 607
 Adriani O., et al., 2016, preprint, ([arXiv:1607.00233](https://arxiv.org/abs/1607.00233))
 Agol E., Kamionkowski M., 2002, *MNRAS*, **334**, 553
 Aguilar M., et al., 2013, *Physical Review Letters*, **110**, 141102
 Aharonian F. A., 2013, *Astroparticle Physics*, **43**, 71
 Aharonian F., et al., 2005, *Science*, **307**, 1938
 Aharonian F., et al., 2006, *ApJ*, **636**, 777
 Aharonian F., et al., 2008, *A&A*, **477**, 353
 Allen S. W., Dunn R. J. H., Fabian A. C., Taylor G. B., Reynolds C. S., 2006, *MNRAS*, **372**, 21
 Armitage P. J., Natarajan P., 1999, *ApJ*, **523**, L7
 Armstrong J. W., Rickett B. J., Spangler S. R., 1995, *ApJ*, **443**, 209
 Arons J., Lea S. M., 1976, *ApJ*, **207**, 914
 Baker J. G., Boggs W. D., Centrella J., Kelly B. J., McWilliams S. T., Miller M. C., van Meter J. R., 2007, *Astrophys. J.*, **668**, 1140
 Bamba A., et al., 2007, *PASJ*, **59**, 209
 Bamba A., Yamazaki R., Kohri K., Matsumoto H., Wagner S., Pühlhofer G., Kosack K., 2009, *ApJ*, **691**, 1854
 Bardeen J. M., Petterson J. A., 1975, *ApJ*, **195**, L65
 Barkov M. V., Khangulyan D. V., Popov S. B., 2012, *MNRAS*, **427**, 589
 Begelman M. C., 2012, *MNRAS*, **420**, 2912
 Begelman M. C., Cioffi D. F., 1989, *ApJ*, **345**, L21
 Bekenstein J. D., 1973, *ApJ*, **183**, 657
 Belczynski K., Holz D. E., Bulik T., O’Shaughnessy R., 2016, *Nature*, **534**, 512
 Berkhuijsen E. M., 1999, in Ostrowski M., Schlickeiser R., eds, *Plasma Turbulence and Energetic Particles in Astrophysics*. pp 61–65
 Binney J., Merrifield M., 1998, *Galactic Astronomy*
 Bird S., Cholis I., Muñoz J. B., Ali-Haïmoud Y., Kamionkowski M., Kovetz E. D., Raccanelli A., Riess A. G., 2016, *Physical Review Letters*, **116**, 201301
 Bisnovatyi-Kogan G. S., Ruzmaikin A. A., 1976, *Ap&SS*, **42**, 401
 Bland-Hawthorn J., Reynolds R., 2000, *Gas in Galaxies*, [doi:10.1888/0333750888/2636](https://doi.org/10.1888/0333750888/2636).
 Blandford R. D., 2000, *Physica Scripta Volume T*, **85**, 191
 Blandford R. D., Begelman M. C., 1999, *MNRAS*, **303**, L1
 Blandford R. D., Begelman M. C., 2004, *MNRAS*, **349**, 68
 Blandford R. D., Znajek R. L., 1977, *MNRAS*, **179**, 433
 Blümer J., Engel R., Hörandel J. R., 2009, *Progress in Particle and Nuclear Physics*, **63**, 293
 Bondi H., 1952, *MNRAS*, **112**, 195

Bondi H., Hoyle F., 1944, *MNRAS*, **104**, 273
 Bonnor W. B., Rotenberg M. A., 1961, *Proceedings of the Royal Society of London Series A*, **265**, 109
 Brandt W. N., Podsiadlowski P., Sigurdsson S., 1995, *Mon. Not. Roy. Astron. Soc.*, **277**, L35
 Campana S., Pardi M. C., 1993, *A&A*, **277**, 477
 Campanelli M., Lousto C. O., Zlochower Y., Merritt D., 2007, *Astrophys. J.*, **659**, L5
 Cao X., 2011, *ApJ*, **737**, 94
 Cardoso V., Macedo C. F. B., Pani P., Ferrari V., 2016, *J. Cosmology Astropart. Phys.*, **5**, 054
 Carr B. J., 1979, *MNRAS*, **189**, 123
 Chevalier C., Ilovaisky S. A., 1998, *A&A*, **330**, 201
 Chisholm J. R., Dodelson S., Kolb E. W., 2003, *ApJ*, **596**, 437
 Cioffi D. F., McKee C. F., Bertschinger E., 1988, *ApJ*, **334**, 252
 Clemens D. P., Sanders D. B., Scoville N. Z., 1988, *ApJ*, **327**, 139
 Connaughton V., et al., 2016, *ApJ*, **826**, L6
 Cordes J. M., Chernoff D. F., 1998, *The Astrophys. J.*, **505**, 315
 Dominik M., et al., 2015, *ApJ*, **806**, 263
 Draine B. T., 2011, *Physics of the Interstellar and Intergalactic Medium*
 Esin A. A., McClintock J. E., Narayan R., 1997, *ApJ*, **489**, 865
 Evans P. A., et al., 2016a, *MNRAS*, **460**, L40
 Evans P. A., et al., 2016b, *MNRAS*, **462**, 1591
 Evoli C., Gaggero D., Grasso D., 2015, *J. Cosmology Astropart. Phys.*, **12**, 039
 Fender R. P., Maccarone T. J., Heywood I., 2013, *MNRAS*, **430**, 1538
 Ferrière K. M., 2001, *Reviews of Modern Physics*, **73**, 1031
 Fitchett M. J., 1983, *MNRAS*, **203**, 1049
 Fujinaga T., et al., 2011, *PASJ*, **63**, S857
 Fujita Y., Inoue S., Nakamura T., Manmoto T., Nakamura K. E., 1998, *ApJ*, **495**, L85
 Fujita Y., Kohri K., Yamazaki R., Ioka K., 2009, *Phys. Rev. D*, **80**, 063003
 Gaisser T. K., Stanev T., Tilav S., 2013, *Frontiers of Physics*, **8**, 748
 Gallo E., Fender R., Kaiser C., Russell D., Morganti R., Oosterloo T., Heinz S., 2005, *Nature*, **436**, 819
 Genolini Y., Putze A., Salati P., Serpico P. D., 2015, *A&A*, **580**, A9
 Goldreich P., Julian W. H., 1969, *ApJ*, **157**, 869
 Gonzalez J. A., Sperhake U., Bruegmann B., Hannam M., Husa S., 2007, *Phys. Rev. Lett.*, **98**, 091101
 Greiner J., Burgess J. M., Savchenko V., Yu H.-F., 2016, *ApJ*, **827**, L38
 Grindlay J. E., 1978, *ApJ*, **221**, 234
 HESS Collaboration et al., 2016, *Nature*, **531**, 476
 Han J. L., Ferriere K., Manchester R. N., 2004, *ApJ*, **610**, 820
 Heckler A. F., Kolb E. W., 1996, *ApJ*, **472**, L85
 Heger A., Fryer C. L., Woosley S. E., Langer N., Hartmann D. H., 2003, *ApJ*, **591**, 288
 Heyer M., Dame T. M., 2015, *ARA&A*, **53**, 583
 Hillas A. M., 2005, *Journal of Physics G Nuclear Physics*, **31**, R95
 Hirotani K., Pu H.-Y., 2016, *ApJ*, **818**, 50
 Hirotani K., Pu H.-Y., Chun-Che Lin L., Chang H.-K., Inoue M., Kong A. K. H., Matsushita S., Tam P.-H. T., 2016, preprint, ([arXiv:1610.07819](https://arxiv.org/abs/1610.07819))
 Hirschi R., Meynet G., Maeder A., 2005, *A&A*, **443**, 581
 Hollenbach D., Johnstone D., Lizano S., Shu F., 1994, *ApJ*, **428**, 654
 Hoyle F., Lyttleton R. A., 1939, *Proceedings of the Cambridge Philosophical Society*, **35**, 405
 Ichimaru S., 1977, *ApJ*, **214**, 840
 Inutsuka S.-i., Inoue T., Iwasaki K., Hosokawa T., 2015, *A&A*, **580**, A49

- Ioka K., 2010, *Progress of Theoretical Physics*, **123**, 743
- Ioka K., Mészáros P., 2010, *ApJ*, **709**, 1337
- Ioka K., Chiba T., Tanaka T., Nakamura T., 1998, *Phys. Rev. D*, **58**, 063003
- Ioka K., Tanaka T., Nakamura T., 1999, *Phys. Rev. D*, **60**, 083512
- Ipser J. R., Price R. H., 1977, *ApJ*, **216**, 578
- Ipser J. R., Price R. H., 1982, *ApJ*, **255**, 654
- Jiang Y.-F., Stone J. M., Davis S. W., 2014, *ApJ*, **796**, 106
- KamLAND Collaboration et al., 2016, preprint, ([arXiv:1606.07155](https://arxiv.org/abs/1606.07155))
- Kashiyama K., Ioka K., Kawanaka N., 2011, *Phys. Rev. D*, **83**, 023002
- Kasliwal M. M., et al., 2016, *ApJ*, **824**, L24
- Kato S., Fukue J., Mineshige S., 2008, *Black-Hole Accretion Disks — Towards a New Paradigm —*
- Kauffmann J., Bertoldi F., Bourke T. L., Evans II N. J., Lee C. W., 2008, *A&A*, **487**, 993
- Kawanaka N., Ioka K., Nojiri M. M., 2010, *ApJ*, **710**, 958
- Kawanaka N., Ioka K., Ohira Y., Kashiyama K., 2011, *ApJ*, **729**, 93
- Kimura S. S., Takahashi S. Z., Toma K., 2016, preprint, ([arXiv:1607.01964](https://arxiv.org/abs/1607.01964))
- Kinugawa T., Inayoshi K., Hotokezaka K., Nakauchi D., Nakamura T., 2014, *MNRAS*, **442**, 2963
- Kinugawa T., Nakano H., Nakamura T., 2016a, preprint, ([arXiv:1606.00362](https://arxiv.org/abs/1606.00362))
- Kinugawa T., Miyamoto A., Kanda N., Nakamura T., 2016b, *MNRAS*, **456**, 1093
- Kinugawa T., Nakano H., Nakamura T., 2016c, *Progress of Theoretical and Experimental Physics*, **2016**, 031E01
- Kobayashi T., Komori Y., Yoshida K., Nishimura J., 2004, *ApJ*, **601**, 340
- Kobulnicky H. A., et al., 2014, *ApJS*, **213**, 34
- Kohri K., Ioka K., Fujita Y., Yamazaki R., 2016, *Progress of Theoretical and Experimental Physics*, **2016**, 021E01
- Koide S., Shibata K., Kudoh T., Meier D. L., 2002, *Science*, **295**, 1688
- Kotera K., Silk J., 2016, *ApJ*, **823**, L29
- Kuijken K., Gilmore G., 1989a, *MNRAS*, **239**, 571
- Kuijken K., Gilmore G., 1989b, *MNRAS*, **239**, 605
- Kulkarni S. R., Hut P., McMillan S., 1993, *Nature*, **364**, 421
- Kyutoku K., Seto N., 2016, *MNRAS*, **462**, 2177
- Lamberts A., Garrison-Kimmel S., Clausen D., Hopkins P., 2016, preprint, ([arXiv:1605.08783](https://arxiv.org/abs/1605.08783))
- Li X., Zhang F.-W., Yuan Q., Jin Z.-P., Fan Y.-Z., Liu S.-M., Wei D.-M., 2016, *ApJ*, **827**, L16
- Lipunov V. M., Kornilov V., Gorbvskoy E., Tiurina N., Balanutsa P., Kuznetsov A., 2016, preprint, ([arXiv:1605.01604](https://arxiv.org/abs/1605.01604))
- Loeb A., 2016, *ApJ*, **819**, L21
- Longair M. S., 2011, *High Energy Astrophysics*
- Lubow S. H., Papaloizou J. C. B., Pringle J. E., 1994, *MNRAS*, **267**, 235
- Lynden-Bell D., 1969, *Nature*, **223**, 690
- Mandel I., de Mink S. E., 2016, *MNRAS*, **458**, 2634
- Mapelli M., 2016, *MNRAS*, **459**, 3432
- Marchant P., Langer N., Podsiadlowski P., Tauris T. M., Moriya T. J., 2016, *A&A*, **588**, A50
- Matsumoto H., et al., 2007, *PASJ*, **59**, 199
- Matsumoto H., et al., 2008, *PASJ*, **60**, S163
- Matsumoto T., Teraki Y., Ioka K., 2016, in preparation
- McDowell J., 1985, *MNRAS*, **217**, 77
- McKinney J. C., Tchekhovskoy A., Blandford R. D., 2012, *MNRAS*, **423**, 3083
- McKinney J. C., Tchekhovskoy A., Blandford R. D., 2013, *Science*, **339**, 49
- Mészáros P., 1975, *A&A*, **44**, 59
- Michel F. C., 1972, *Ap&SS*, **15**, 153
- Miller-Jones J. C. A., 2014, *Publ. Astron. Soc. Australia*, **31**, e016
- Mirabel I. F., Rodrigues I., 2003, *Science*, **300**, 1119
- Mirabel I. F., Dhawan V., Mignani R. P., Rodrigues I., Guglielmetti F., 2001, *Nature*, **413**, 139
- Mirabel I. F., Mignani R., Rodrigues I., Combi J. A., Rodríguez L. F., Guglielmetti F., 2002, *A&A*, **395**, 595
- Mizuta A., Ioka K., 2013, *ApJ*, **777**, 162
- Morokuma T., et al., 2016, *PASJ*, **68**, L9
- Morsony B. J., Workman J. C., Ryan D. M., 2016, *ApJ*, **825**, L24
- Murase K., Kashiyama K., Mészáros P., Shoemaker I., Senno N., 2016, *ApJ*, **822**, L9
- Nakamura T., Sasaki M., Tanaka T., Thorne K. S., 1997, *ApJ*, **487**, L139
- Nakamura T., Nakano H., Tanaka T., 2016a, *Phys. Rev. D*, **93**, 044048
- Nakamura T., et al., 2016b, *Progress of Theoretical and Experimental Physics*, **2016**, 093E01
- Nakano T., Nishi R., Umebayashi T., 2002, *ApJ*, **573**, 199
- Narayan R., Yi I., 1994, *ApJ*, **428**, L13
- Narayan R., Yi I., 1995, *ApJ*, **452**, 710
- Narayan R., Iğumenshchev I. V., Abramowicz M. A., 2003, *PASJ*, **55**, L69
- Norman C. A., Melrose D. B., Achterberg A., 1995, *ApJ*, **454**, 60
- Novikov I. D., Thorne K. S., 1973, in Dewitt C., Dewitt B. S., eds, *Black Holes (Les Astres Occlus)*. pp 343–450
- Ohsuga K., Mineshige S., 2011, *ApJ*, **736**, 2
- Ohsuga K., Mori M., Nakamoto T., Mineshige S., 2005, *ApJ*, **628**, 368
- Oliva A., 2016, *PoS, ICRC2015*, 265
- Palliyaguru N. T., et al., 2016, preprint, ([arXiv:1608.06518](https://arxiv.org/abs/1608.06518))
- Peres A., 1962, *Physical Review*, **128**, 2471
- Perna R., Lazzati D., Giacomazzo B., 2016, *ApJ*, **821**, L18
- Pfahl E., Rappaport S., Podsiadlowski P., Spruit H., 2002, *The Astrophys. J.*, **574**, 364
- Portegies Zwart S. F., McMillan S. L. W., 2000, *ApJ*, **528**, L17
- Pringle J. E., Rees M. J., 1972, *A&A*, **21**, 1
- Racusin J. L., et al., 2016, preprint, ([arXiv:1606.04901](https://arxiv.org/abs/1606.04901))
- Rafferty D. A., McNamara B. R., Nulsen P. E. J., Wise M. W., 2006, *ApJ*, **652**, 216
- Ramirez-Ruiz E., Celotti A., Rees M. J., 2002, *MNRAS*, **337**, 1349
- Reid M. J., McClintock J. E., Narayan R., Gou L., Remillard R. A., Orosz J. A., 2011, *The Astrophys. J.*, **742**, 83
- Remillard R. A., McClintock J. E., 2006, *ARA&A*, **44**, 49
- Repetto S., Davies M. B., Sigurdsson S., 2012, *Mon. Not. Roy. Astron. Soc.*, **425**, 2799
- Rodriguez C. L., Morscher M., Pattabiraman B., Chatterjee S., Haster C.-J., Rasio F. A., 2015, *Physical Review Letters*, **115**, 051101
- Rodriguez C. L., Chatterjee S., Rasio F. A., 2016, *Phys. Rev. D*, **93**, 084029
- Russell H. R., McNamara B. R., Edge A. C., Hogan M. T., Main R. A., Vantyghe A. N., 2013, *MNRAS*, **432**, 530
- Sakai M., Yajima Y., Matsumoto H., 2011, *PASJ*, **63**, S879
- Salpeter E. E., 1964, *ApJ*, **140**, 796
- Sana H., et al., 2012, *Science*, **337**, 444
- Sasaki M., Suyama T., Tanaka T., Yokoyama S., 2016, *Physical Review Letters*, **117**, 061101
- Savchenko V., et al., 2016, *ApJ*, **820**, L36
- Śądowski A., Narayan R., McKinney J. C., Tchekhovskoy A., 2014, *MNRAS*, **439**, 503
- Śądowski A., Lasota J.-P., Abramowicz M. A., Narayan R., 2016, *MNRAS*, **456**, 3915
- Scoville N. Z., Sanders D. B., 1987, in Hollenbach D. J., Thronson Jr. H. A., eds, *Astrophysics and Space Science Library Vol. 134, Interstellar Processes*. pp 21–50
- Serpico P. D., 2012, *Astroparticle Physics*, **39**, 2

Sesana A., 2016, *Physical Review Letters*, **116**, 231102
 Shakura N. I., Sunyaev R. A., 1973, *A&A*, **24**, 337
 Shapiro S. L., 1973, *ApJ*, **180**, 531
 Shapiro S. L., Teukolsky S. A., 1983, Black holes, white dwarfs, and neutron stars: The physics of compact objects
 Shvartsman V. F., 1971, *Soviet Astr.*, **15**, 377
 Sigurdsson S., Hernquist L., 1993, *Nature*, **364**, 423
 Tavani M., et al., 2016, *ApJ*, **825**, L4
 Tchekhovskoy A., Narayan R., McKinney J. C., 2011, *MNRAS*, **418**, L79
 Teraki Y., Matsumoto T., Ioka K., 2016, in preparation
 The LIGO Scientific Collaboration et al., 2016, preprint, ([arXiv:1606.04856](https://arxiv.org/abs/1606.04856))
 The Pierre Auger Collaboration et al., 2016, preprint, ([arXiv:1608.07378](https://arxiv.org/abs/1608.07378))
 Troja E., Read A. M., Tiengo A., Salvaterra R., 2016, *ApJ*, **822**, L8
 Tutukov A. V., Yungelson L. R., 1993, *MNRAS*, **260**, 675
 Veres P., Preece R. D., Goldstein A., Mészáros P., Burns E., Connaughton V., 2016, *ApJ*, **827**, L34
 Waxman E., 2004, *Pramana*, **62**, 483
 White N. E., van Paradijs J., 1996, *Astrophys. J. Letter*, **473**, L25
 Yamazaki R., Kohri K., Bamba A., Yoshida T., Tsuribe T., Takahara F., 2006, *MNRAS*, **371**, 1975
 Yamazaki R., Asano K., Ohira Y., 2016, *Progress of Theoretical and Experimental Physics*, **2016**, 051E01
 Yoon S.-C., Langer N., 2005, *A&A*, **443**, 643
 Yuan F., Narayan R., 2014, *ARA&A*, **52**, 529
 Yuan F., Gan Z., Narayan R., Sadowski A., Bu D., Bai X.-N., 2015, *ApJ*, **804**, 101
 Zamaninasab M., Clausen-Brown E., Savolainen T., Tchekhovskoy A., 2014, *Nature*, **510**, 126
 Zel'dovich Y. B., 1964, *Soviet Physics Doklady*, **9**, 195
 Zhang B., 2016, *ApJ*, **827**, L31
 Zlochower Y., Lousto C. O., 2015, *Phys. Rev.*, D92, 024022
 de Jager O. C., et al., 2009, preprint, ([arXiv:0906.2644](https://arxiv.org/abs/0906.2644))

APPENDIX A: COMPARISON WITH PREVIOUS WORKS

Studying the accreting BHs in our Galaxy has a long history from 1920's Eddington era. However the observations of GWs set a lower limit on the number of spinning BHs for the first time. Our paper gives the first considerations on the Galactic BHs after the discovery of GWs.

Hoyle & Lyttleton (1939) considered the effect of the ISM accretion on the Sun's radiation for explaining changes in terrestrial climate. Bondi & Hoyle (1944) investigated the accretion in detail including the effect of perturbations. Bondi (1952) included the pressure effects to complete the Bondi-Hoyle formula.

Zel'dovich (1964) and Salpeter (1964) suggested accretion onto a BH as an important source of radiation. Shvartsman (1971) treated both the fluid dynamics and radiative processes by employing nonrelativistic approximations. Michel (1972) considered the general-relativistic version of the Bondi-Hoyle accretion. Shapiro (1973) made a general-relativistic treatment of both the fluid mechanics and radiative processes. Mészáros (1975) included the heating due to dissipation of turbulence and magnetic reconnection, and the radiation from cosmic rays captured with the accretion.

The formation of a disk around a massive BH is considered by Lynden-Bell (1969). Pringle & Rees (1972) developed the accretion disk model. Shakura & Sunyaev (1973) completed the standard disk model. Novikov & Thorne (1973) made a general-relativistic version of the standard disk model.

Ipser & Price (1977, 1982) carried out detail calculations of radiation from Galactic massive BHs that are spherically accreting from the ISM. Grindlay (1978) discussed X-ray limits on Galactic BHs that are spherically accreting from the ISM. Carr (1979) placed a limit on BHs with the background radiation density. McDowell (1985) suggested that molecular clouds offer high density for spherically accreting BHs to produce detectable fluxes. Campana & Pardi (1993) estimated the number of BHs in the molecular clouds. Heckler & Kolb (1996) proposed a search strategy for isolated stellar mass BHs in the solar neighborhood using optical surveys. Chisholm et al. (2003) gave possible BH candidates using optical and X-ray surveys.

Modern estimates for radiation from isolated stellar mass BHs began after Fujita et al. (1998) adopted the advection-dominated accretion flow (ADAF) model and Armitage & Natarajan (1999) considered a jet from an isolated accreting BH, although they do not estimate the luminosity function, the total power, and the acceleration energy. They did not also consider the MAD state.

Agol & Kamionkowski (2002) calculated the luminosity function of isolated accreting BHs, although they assumed a constant efficiency of the disk emission and do not consider a BH jet.

Barkov et al. (2012) also considered a jet from an isolated accreting BH, although they do not consider the luminosity function and hence their estimate on the total power is not correct. They did not also consider the MAD state.

Fender et al. (2013) calculated the X-ray luminosity distribution and suggested a discrepancy between the theoretical expectation and the hard X-ray surveys, although their prescription for radiatively inefficient accretion is very simple.

Nakamura et al. (2016a) considered the Bondi-Hoyle accretion for the optical counterparts of nearby BH mergers.

This paper has been typeset from a $\text{\TeX}/\text{\LaTeX}$ file prepared by the author.